SAMHD1 promotes SARS-CoV-2 infection by enhancing HNF1-dependent ACE2 expression in lung epithelial cells

Short title: SAMHD1 promotes SARS-CoV-2 entry via HNF1-dependent ACE2 expression

Pak-Hin Hinson Cheung[1,#], Pearl Chan[1], Hua Yang[1], Shravya Honne[2], Baek Kim[2], Stanley Perlman[1], Li Wu[1,#]

[1] Department of Microbiology and Immunology, Carver College of Medicine, University of Iowa, Iowa City, Iowa, USA,

[2] Department of Pediatrics, School of Medicine, Emory University, Atlanta, Georgia, USA

Address correspondence to Pak-Hin Hinson Cheung (pakhinhinson-cheung@uiowa.edu) or Li Wu (li-wu@uiowa.edu).

Keywords: SAMHD1, SARS-CoV-2, replication, entry, HNF1, ACE2, Calu-3 cells

Manuscript information:

- 9 main figures, 5 supplementary figures, and 5 supplementary tables
- 258 words in the abstract and 150 words in the author summary

Abstract

Sterile alpha motif and HD domain-containing protein 1 (SAMHD1) restricts a board spectrum of viruses through multifaceted mechanisms. It also limits spontaneous- and virus-induced innate immune responses by suppressing proinflammatory cytokine and type-I interferon (IFN-I) production. Some viruses escape SAMHD1 restriction by utilizing SAMHD1-mediated innate immune suppression to establish effective infection through viral antagonism. Our previous studies showed that SAMHD1 is a proviral factor facilitating replication of severe acute respiratory syndrome coronavirus (SARS-CoV-2) in human macrophages, monocytic THP-1 and epithelial-like HEK293T cell lines by suppressing IFN responses. However, it is unclear about the function of SAMHD1 in lung epithelial cells during SARS-CoV-2 infection. Here, we report that SAMHD1 facilitates SARS-CoV-2 replication in lung epithelial Calu-3 cells by enhancing endogenous expression of the viral receptor angiotensin-converting enzyme 2 (ACE2) via hepatocyte nuclear factor 1-alpha (HNF1α) and HNF1β. Using pseudotyped SARS-CoV-2 and lentiviral vectors, we found that SARS-CoV-2 spike protein-mediated viral entry was suppressed in Calu-3 cells with SAMHD1 knockout (KO). SAMHD1 KO repressed ACE2 expression in Calu-3 cells at mRNA and protein levels. Functional analyses revealed that HNF1α and HNF1β were crucial for the endogenous ACE2 expression in Calu-3 cells. Additionally, SAMHD1 KO led to a reduction in the expression levels and ACE2-promoting function of HNF1α and HNF1β. Inhibition of IFN antiviral

response by baricitinib, a Janus kinase 1 and 2 (JAK 1/2) inhibitor, did not revert the suppression of SARS-CoV-2 in SAMHD1 KO Calu-3 cells. Our findings demonstrate that SAMHD1 facilitates HNF1-mediated ACE2 expression and SARS-CoV-2 replication in Calu-3 cells via a novel mechanism beyond its IFN-suppressive function.

Author Summary

During viral infection, SAMHD1 acts as a viral restriction factor and a suppressor of the innate immune system, controlling viral replication while also ensuring immune homeostasis. The innate immune suppressive function of SAMHD1 can be proviral for some viruses. SAMHD1 has been shown to facilitate SARS-CoV-2 infection in human macrophages, THP-1 and HEK293T cell lines by promoting IFN antagonism, but its role in lung epithelial cells is unclear. Here, we demonstrated that SAMHD1 promotes SARS-CoV-2 replication in human lung epithelial Calu-3 cells by enhancing expression of the major viral receptor ACE2. We found that SAMHD1 facilitated HNF1-medaited ACE2 expression that was required for spike protein-mediated SARS-CoV-2 entry. However, inhibiting IFN signaling in SAMHD1 KO Calu-3 cells was not sufficient to revert SARS-CoV-2 replication. Our findings shed light on the differential proviral function of SAMHD1 in ACE2 expressing cells and suggest that SAMHD1 can facilitate SARS-CoV-2 infection beyond enhancing IFN antagonism.

55

56 **Introduction**

57 SAMHD1 is the only deoxynucleoside triphosphohydrolase (dNTPase) of mammalian cells
58 to be a restriction factor against human immunodeficient virus type 1 (HIV-1) infection in resting
59 $CD4^+$ T cells and terminally differentiated immune cells, such as macrophages and dendritic cells
60 [1-3]. Increasing evidence suggests that SAMHD1 restricts different viruses including human T
61 cell leukemia virus type 1 [4], DNA viruses such as herpesviruses (herpes simplex virus 1, human
62 cytomegalovirus and Epstein-Barr virus), hepatitis B virus, human papillomavirus and poxviruses
63 [5-10] as well as RNA viruses including influenza A virus, enteroviruses, and flaviviruses [11-13].
64 The viral restriction functions of SAMHD1 encompass both dNTPase-dependent and -
65 independent mechanisms according to the target virus and the contexts of the host cells such as
66 cell type, differentiation status, IFN-I response and the expression of other host restriction factors
67 that cooperate with SAMHD1 in cells [14].

68 SAMHD1 suppresses innate immune responses [15]. Loss-of-function mutation of SAMHD1
69 correlates with the development of the Aicardi-Goutières syndrome which is an autoimmune
70 disease implicating central nervous system [16]. SAMHD1 prevents spontaneous activation of
71 innate immune responses to self-RNA and self-DNA species that respectively activate retinoic
72 acid-inducible gene I (RIG-I)-like receptor signaling and cyclic GMP-AMP synthase (cGAS)-

73 stimulator of interferon genes (STING) signaling [17-24]. Similarly, SAMHD1 prevents
74 inflammation- or virus-induced innate immune responses [25, 26]. SAMHD1 suppresses pattern
75 recognition receptor signal pathways by interacting with various signal proteins such as
76 mitochondrial antiviral-signaling protein (MAVS), inhibitor of nuclear factor kappa-B kinase subunit
77 alpha (IKKα), IKKβ, IKKε as well as transcription factors including p100 and p105 in the NF-κB
78 pathway which drives proinflammatory cytokine expression and interferon regulatory factor 7
79 (IRF7) which promotes IFN-I expression [25, 27, 28].

80 SARS-CoV-2 caused the COVID-19 pandemic, claiming more than 7 million lives worldwide
81 [29, 30]. SARS-CoV-2 suppresses IFN antiviral responses through multiple strategies to facilitate
82 viral infection [31]; however, the precise mechanisms remain to be elucidated. Previously, we
83 reported that SARS-CoV-2 infection was suppressed upon depletion of SAMHD1 expression in
84 HEK293T, differentiated THP-1 cells, and primary human macrophages [32]. Suppression of IFN
85 signaling of SAMHD1-defective HEK293T cells by baricitinib, a JAK1/2 inhibitor, alleviated the
86 repression of SARS-CoV-2 replication, suggesting that SARS-CoV-2 exploits SAMHD1 for IFN
87 antagonism, thereby facilitating its infection [32]. It remains to be determined if SAMHD1-
88 mediated immunosuppression promotes SARS-CoV-2 replication in the primary target cell type,
89 such as epithelial cells expressing the major viral entry factors ACE-2 and transmembrane
90 protease, serine 2 (TMPRSS2) [33, 34].

91 In this study, we found that SAMHD1 KO in Calu-3 cells conferred resistance to SARS-CoV-
92 2 infection, independent of IFN signaling, by reducing the expression of transcription factors
93 HNF1α and HNF1β, which in turn lowered ACE2 levels and inhibited S-mediated viral entry. Our
94 findings shed light on a novel function of SAMHD1 in upregulating ACE2 expression to facilitate
95 SARS-CoV-2 infection in human lung epithelial cells.
96

97 **Results**

98 **Generation and characterization of stable SAMHD1 KO Calu-3 cell lines**

99 To generate SAMHD1 KO Calu-3 cells, CRISPR/Cas9 technology based on the
100 lentiCRISPRv2 system was employed [35]. Two target sequences of the single guide RNAs
101 (sgRNAs) were obtained from CHOPCHOP v3 with no off-target effect at less than four
102 mismatches [36]. With sgRNA 1 and sgRNA 2, the *Streptococcus pyogenes* Cas9 nuclease
103 (SpCas9) was targeted to the SAMHD1 gene, resulting in cleavage sites that encode ^{11}Lysine and
104 ^{150}Leucine, respectively (Fig. 1A). ^{11}Lysine was the first residue of the nuclear localizing signal
105 (NLS) of SAMHD1 protein and ^{150}Leucine was in the HD domain before the dNTPase active site.
106 Calu-3 cells were transduced with the lentiviral vectors, selected by puromycin and clonal
107 purified with limiting dilution. Several purified cell clones were obtained and tested for SAMHD1
108 protein expression (Fig. 1B). We obtained clone 4 and clone 3 of the respective cell populations

109 treated with sgRNA1 or sgRNA2 having the lowest expression of SAMHD1 compared with the
110 Ctrl clones (Fig. 1B). Therefore, clone 1 of the Ctrl population, clone 4 of the sgRNA1-treated
111 population and clone 3 of the sgRNA2-treated population were used for the subsequent study
112 and named Ctrl, KO1 and KO2, respectively.

113 The genomic DNA sequences at the SpCas9 cleavage sites of KO1 cells (Fig. S1A) and KO2
114 cells (Fig. S1B) were obtained through sanger sequencing and compared with Ctrl cells. We found
115 that a single nucleotide insertion occurred near the SpCas9 cleavage sites, which frameshifted
116 the SAMHD1 coding sequence thereafter (Red arrows, Fig. S1A and S1B). It was noted that
117 multiple signal peaks were observed after the SpCas9 cleavage sites of KO1 and KO2 which may
118 indicate the existence of more than one mutant in the clonal purified population.

119 To confirm whether SAMHD1 KO functionally affected intracellular dNTP levels, cellular
120 dATP levels were measured (Fig. S1C) as an example [37]. We found that the mean values of
121 the intracellular dATP levels of KO1 and KO2 were 8.9- and 7.8- fold more than that of the Ctrl
122 cells (Fig. S1C). This result suggests that KO1 and KO2 were deprived of dNTPase activity of
123 SAMHD1.

124 SAMHD1 depletion may enhance innate immune response even in the absence of extrinsic
125 stimuli depending on cell types [19, 24, 25, 32, 38-40]. To examine if SAMHD1 KO promoted
126 innate immune responses of Calu-3 cells, the mRNA levels of proinflammatory cytokine *IL-6* as

127 well as *IFNβ* and two IFN-stimulated genes (ISGs) *OAS1* and *ISG15* of KO1 and KO2 were
128 detected by RT-qPCR and compared with Ctrl cells (Fig. 1C). We found that KO1 and KO2 cells
129 constitutively expressed higher levels of IL-6 in the absence of any extrinsic stimuli. Interestingly,
130 we found that the expression levels of *IFNβ*, *OAS1* and *ISG15* were significantly upregulated in
131 KO2, but not in KO1 clone (Fig. 1C). Thus, SAMHD1 KO promoted proinflammatory cytokine
132 production from Calu-3 cells in both KO1 and KO2 clones, while strong constitutive IFN-I response
133 was only observed in KO2 clone.

134 **SAMHD1 promotes SARS-CoV-2 replication independent of IFN signaling**

135 To test if SAMHD1 affected SARS-CoV-2 replication in Calu-3 cells, kinetics of ancestral
136 SARS-CoV-2 (Wuhan-Hu-1) replication was examined in Ctrl, KO1 and KO2 cells. We found that
137 the kinetics of infectious virus production was suppressed in both KO1 and KO2 (Fig. 2A) despite
138 only KO2 cells having a higher constitutive IFN-I response than Ctrl cells (Fig. 1C). Similarly,
139 significant suppression of the levels of released viral genome was observed in both KO1 and KO2
140 clones (Fig. 2B). The expressions of intracellular viral nucleoprotein (N) and spike protein (S) were
141 significantly reduced in the infected KO1 and KO2 cells (Fig. 2C). Moreover, intracellular viral RNA
142 levels were suppressed in the infected KO1 and KO2 cells which did not produce higher levels of
143 IFNβ, IFNλ or OAS1 in response to SARS-CoV-2 infection (Fig. 2D). To confirm if IFN signaling
144 contributed to the hindered replication of SARS-CoV-2 in SAMHD1 KO Calu-3 cells, infected cells

145 were treated with or without baricitinib to test if suppressing IFN signaling can rescue SARS-CoV-
146 2 replication in KO1 and KO2 cells. We found that baricitinib did not rescue SARS-CoV-2
147 replication in Calu-3 cells in terms of released infectious viral titer (Fig. 2E), intracellular viral N
148 protein (Fig. 2F), and intracellular viral *N* mRNA, although baricitinib efficiently suppressed virus-
149 induced *OAS1* expression in Ctrl and KO2 cells (Fig. 2G) as well as virus-induced protein
150 expression of STAT1 and Ser727-phosphorylated STAT1 (Fig. 2F). Therefore, SAMHD1
151 expression is required for SARS-CoV-2 replication in Calu-3 cells independent of its suppressive
152 function to IFN.

153 **SAMHD1 facilitates spike protein-mediated viral entry of SARS-CoV-2**

154 To understand how SAMHD1 promoted SARS-CoV-2 infection, we employed a previously
155 developed single cycle SARS-CoV-2 which was S-defective and pseudotyped with vesicular
156 stomatitis virus glycoprotein (VSV-G), namely, ΔS-VRP(G) [41]. ΔS-VRP(G) infection bypasses
157 S-protein mediated viral entry and infects cell types that do not support authentic SARS-CoV-2
158 infection. Firstly, we confirmed that remdesivir, a nucleoside analogue inhibiting viral RNA-
159 dependent RNA polymerase (RdRP) [42], can efficiently suppress intracellular viral RNA levels (N
160 and E genes) of ΔS-VRP(G) in Calu-3 Ctrl cells, suggesting that ΔS-VRP(G) infection depended
161 on RdRP activity (Fig. 3A). Next, we asked if SAMHD1 deficiency suppressed ΔS-VRP(G)
162 infection similarly as that observed in the authentic SARS-CoV-2 infections (Fig. 2). Interestingly,

163 we found that the intracellular viral N and E RNA levels of ΔS-VRP(G) were not suppressed in
164 KO1 or KO2 cells compared with Ctrl cells at 24 and 48 hrs post-infection (hpi) (Fig. 3B).
165 Comparatively, we observed that intracellular viral N protein expression by ΔS-VRP(G) infection
166 was minimally affected in KO1 cells but was slightly reduced in KO2 cells (Fig. 3C), although the
167 difference was much less than that observed in the authentic SARS-CoV-2 infection (Fig. 2C).
168 ΔS-VRP(G) expresses a dual reporter gene (*Gaussia* luciferase-T2A-neon GFP) through the
169 transcriptional regulatory sequence of S gene [41]. Detection to the *Gaussia* luciferase activity
170 reflects the infectivity of ΔS-VRP(G) [41]. We found that ΔS-VRP(G) infection produced similar
171 levels of *Gaussia* luciferase in Ctrl, KO1 and KO2 cells (Fig. 3D). Although ΔS-VRP(G) infection
172 had a trend of producing less *Gaussia* luciferase in KO2 cells than KO1 and Ctrl, we did not
173 observe significant reductions in both KO1 and KO2 cells (Fig. 3D). Therefore, unlike authentic
174 SARS-CoV-2, SAMHD1 deficiency did not inhibit ΔS-VRP(G) infection.

175 One possible explanation for the selective suppression of authentic SARS-CoV-2 infection
176 but not ΔS-VRP(G) in SAMHD1 KO cells was due to abolished S-protein-mediated viral entry,
177 which was not required for ΔS-VRP(G) infection. To validate the possibility, we employed a SARS-
178 CoV-2 S protein-pseudotyped HIV-1-based reporter virus, namely HIV-1-spike-Luc/ZsGreen [43,
179 44]. Successful infection of HIV-1-spike-Luc/ZsGreen depended on S-protein mediated viral entry
180 and the subsequent viral gene expression driven by HIV-1 single-cycle infection. The infectivity of

181 HIV-1-spike-Luc/ZsGreen can be measured by detecting the expression of the firefly luciferase 2

182 [43, 44]. We found that HIV-1-spike-Luc/ZsGreen infected KO1 or KO2 cells produced significantly

183 less luciferase activity than the Ctrl cells (Fig. 3E). This suggested that SAMHD1 expression

184 promoted S protein-mediated viral entry, which in turn facilitated infection of authentic SARS-CoV-

185 2 and HIV-1-spike-Luc/ZsGreen but not ΔS-VRP(G).

186 **SAMHD1 maintains the expression of viral receptor ACE2 of Calu-3 cells**

187 To gain mechanistic insight into how SAMHD1 facilitated spike-protein mediated viral entry,

188 the transcriptomic profiles of Ctrl, KO1 and KO2 cells were obtained by mRNA-Sequencing

189 (mRNA-seq). Firstly, principal component analysis (PCA) was performed to cluster Ctrl, KO1 and

190 KO2 cells. Biological triplicate experiment was performed. Nine PCs were therefore obtained, in

191 which PC1 (61%) and PC2 (37%) covered 98% of the total variance (Fig. S2A). Ctrl, KO1 and

192 KO2 cells were well clustered based on PC1 and PC2 (Fig. S2B). Along PC1 axis, KO1 and KO2

193 cells were clearly clustered and separated from Ctrl cells in the same direction. KO2 cells were

194 separated from KO1 and Ctrl cells along the PC2 axis which however minimally distinguished

195 KO1 and Ctrl cells, suggesting clonal specific transcriptomic profile for KO2.

196 A PCA biplot on the top ten most influential loading genes for the PCA clustering was plotted

197 (Fig. S2C). The PCA biplot indicated that the major loading contributors of PC1 were cell surface

198 proteins (CEACAM6, LGALS4 (or Galectin 4), and GJA1) and proteins implicating extracellular

199 matrix (CST6 (Cystatin E/M) and FAM20C). For PC2, the expression changes of ISGs including
200 OAS2, IFI27, IFITM1 and IF16 as well as MHC class II β-chain component HLA-DPB1
201 distinguished KO2 from Ctrl and KO1 but had minimal contribution to PC1 axis (Fig. S2C). In
202 summary, KO1 and KO2 were distinguished from Ctrl along PC1 which was mainly influenced by
203 the mRNA expression of genes implicating cell surface and extracellular matrix while KO2 was
204 further distinguished from Ctrl and KO1 along PC2 which was mainly influenced by the
205 expressions of ISGs.

206 Next, by analyzing the differential expressed genes (DEGs) implicated in both KO1 and KO2
207 having more than 2-fold change and with false discovery rate (FDR)-adjusted P values < 0.01
208 (Table S1), we found that 806 DEGs were commonly observed in KO1 and KO2 compared with
209 Ctrl cells (Fig. 4A). Among the 806 DEGs, 681 DEGs were of the same direction of change (Table
210 S2). We searched for known and validated entry factors of SARS-CoV-2 infection. We found that
211 the expressions of ACE2 and TMPRSS2 were decreased in both KO1 and KO2 (Fig. 4B). Both
212 ACE2 and TMPRSS2 transcripts were more suppressed in KO1 than in KO2. Other known SARS-
213 CoV-2 entry factors were, however, not on the list. Those included alternative receptors
214 Transmembrane protein 106B (TMEM106B) [45], transferrin receptor [46], CD147 [47], AXL
215 receptor tyrosine kinase (AXL) [48], kringle containing transmembrane protein 1 (KREMEN1), and
216 asialoglycoprotein receptor 1 (ASGR1) [49], attachment factors Neuropilin-1 [50], Niemann-Pick

217 C1 (NPC1) [51], lectin receptors [52], and endosomal protease cathepsin L [53] (Table S2).
218 Interestingly, we noticed both KO1 and KO2 had enhanced expression of furin protease (Fig. 4B),
219 which may facilitate S protein priming in infected cells [54].

220 Finally, ACE2 and TMPRSS2 mRNA and protein expressions were validated respectively by
221 RT-qPCR (Fig. 4C) and Western blot (Fig. 4D). For ACE2, we designed a primer pair targeting
222 the full-length isoforms but not the N-terminally truncated ACE2 (dACE2) that is not a functional
223 receptor to SARS-CoV-2 [55]. We employed a monoclonal ACE2 antibody that detected an N-
224 terminal region (peptide sequence surrounding Asp201) that is absent in dACE2. For TMRPSS2,
225 we designed a primer pair that can detect isoform 1 to 3. We employed a monoclonal TMPRSS2
226 antibody that detected the protease domain which is present in both zymogen (~ 55 kDa) and
227 active form (~ 31 kDa).

228 We found that the full length ACE2 mRNA and protein expressions were significantly reduced
229 in KO1 and KO2 cells (Fig. 4C and 4D). We confirmed the decreased full length ACE2 mRNA
230 expression in KO1 and KO2 by another qPCR primer pair [55] (Fig. S3A). Interestingly, we found
231 that KO2, but not KO1 cells, expressed significantly higher levels of dACE2 (Fig. S3B), which is
232 known to be induced by IFN-I [55, 56]. In contrast, we found that TMPRSS2 mRNA and protein
233 expressions were only downregulated in KO1 but not in KO2 cells (Fig. 4C and 4D). Indeed,
234 mRNA-seq results showed that TMPRSS2 transcripts were marginally defined as DEG in KO2

235 cells with log_2 fold change equal to -1.01 (Fig. 4B, right panel). Therefore, only the expression of
236 full-length ACE2 but not TMPRSS2 was confirmed to be commonly repressed in SAMHD1 KO
237 Calu-3 cells. This suggested that SAMHD1 expression was important to maintain full length ACE2
238 expression that facilitated S protein-mediated viral entry and SARS-CoV-2 infection.

239 **SAMHD1 expression does not affect ACE2 mRNA stability**

240 ACE2 mRNA levels were downregulated in SAMHD1 KO cells (Fig. 4B-4C, S3A). To test
241 whether SAMHD1 KO affected ACE2 mRNA stability, an actinomycin D (actD) treatment assay
242 was performed [57, 58]. Ctrl, KO1 and KO2 cells were treated with actD that inhibited transcription.
243 At various time points following the treatment, the ACE2 mRNA levels were measured by three
244 specific qPCR primer pairs: the same qPCR primer pair used in Fig. 4C for full length ACE2
245 targeting exon 2/3 junction and exon 4 (Fig. 5A, primer pair 1 in Table S5), a qPCR primer pair
246 targeting the 5' end of ACE2 mRNA at exon 1/2 junction (Fig. 5B, primer pair 2 in Table S5), and
247 a qPCR primer pair targeting the 3' end of ACE2 mRNA at exon 19 (Fig. 5C, primer pair 3 in Table
248 S5). We found that ACE2 mRNA was relatively stable over time that more than 50% of it remained
249 by 8 hrs of actD treatment (Fig. 5A-5C), similar to the observation by others [59].

250 We included additional controls to validate the actD treatment assay. The mRNA stability of
251 a proapoptotic gene BCL-2 interacting killer (BIK) is suppressed by La-related protein 1 (LARP1),
252 a protein highly expressed in cancer cells [60, 61]. We found that BIK mRNA in Calu-3 Ctrl cells

253 exhibited rapid decay following actD treatment, with levels decreasing to below 50% by 4 hrs and
254 approximately 10% remaining at 8 hrs (Fig. 5D). Comparatively, 18S ribosomal RNA, which is a
255 structural component of ribosome and more stable than mRNA, was found to remain above 50%
256 of the initial levels during the actD treatment assay (Fig. 5E). These results confirmed that the
257 actD treatment assay was valid in distinguishing unstable RNA species. We found that ACE2
258 mRNA in actD-treated KO1 or KO2 cells were similarly stable as compared with that of the Ctrl
259 cells with over 50% of *ACE2* mRNA remaining in both KO1 and KO2 cells (Fig. 5A-5C). Therefore,
260 SAMHD1 expression does not affect ACE2 mRNA stability.

261 **SAMHD1 maintains HNF1α, HNF1β and HNF4α expressions in Calu-3 cells**

262 Next, we questioned how SAMHD1 KO affected *ACE2* transcription. The *ACE2* promoter is
263 a bipartite promoter that is controlled by various transcription factors depending on cell types [62].
264 Analysis of human lung tissues and immortalized lung 16HBE cells revealed STAT3
265 transcriptionally controlled ACE2 expression [63]. HNF1α and HNF1β were found to cooperate
266 and promote ACE2 expression transcriptionally in HEK293 and pancreatic islet cells [64, 65].
267 HNF4α was found to be a transcription repressor or activator of ACE2 expression depending on
268 different cell types and experiment settings [66-68]. Sp1 was found to transcriptionally promote
269 ACE2 expression in immortalized human type II alveolar epithelial cells [68]. FOXA2 was found
270 to promote ACE2 transcription in 832/13 insulinoma cells or mouse pancreatic islets [69]. Ikaros

271 was found to drive ACE2 expression in human cardiac fibroblasts in response to Ang II stimulation
272 by binding to ATTTGGA sequence of the proximal promoter [70].

273 The exact transcription factors regulating endogenous ACE2 expression in Calu-3 cells
274 remain unclear. To the best of our knowledge, GATA6 was the only experimentally identified
275 transcription factor in Calu-3 cells promoting ACE2 expression and facilitating SARS-CoV-2
276 infection [71]. GATA6 was identified by CRISPR/Cas9-KO library screening for surviving cells
277 upon SARS-CoV-2 infection. Two additional independent studies identified HNF1β as a significant
278 candidate to reduce surviving cells upon SARS-CoV-2 infection by CRISPR/Cas9-activation
279 library screening [72, 73]. However, unlike GATA6, the role of HNF1β in regulating ACE2
280 expression in Calu-3 cells was not further validated. Other known ACE2 transcription factors as
281 mentioned above were not on the candidate list of the three screening studies [71-73]. Our RT-
282 qPCR analysis revealed that the mRNA levels of HNF1β were reduced in KO1 and KO2 cells (Fig.
283 6B), while GATA6 mRNA level was unchanged in KO1 and KO2 cells compared to Ctrl cells (Fig.
284 6D).

285 HNF1α, HNF1β, and HNF4α are core transcription factors that establish a complex and
286 interdependent regulatory network during liver and pancreas development [74, 75]. Particularly in
287 hepatocytes, HNF1α and HNF1β can transcriptionally promote the expression of HNF4α [76]. In
288 return, HNF4α promotes HNF1α's expression [77, 78] and transcriptional activity [79]. This

289 network in lung cells is unclear. We found that the mRNA levels of HNF1α (Fig. 6A) and HNF4α
290 (Fig. 6C) were also downregulated in KO1 and KO2 cells. Western blot analysis showed that the
291 protein levels of HNF1α, HNF1β and HNF4α were reduced in KO1 and KO2 cells compared to
292 Ctrl cells (Fig. 6E). These results suggest that endogenous SAMHD1 maintains the expression of
293 the HNF1α, HNF1β and HNF4α in Calu-3 cells.

294 **HNF1α and HNF1β promote endogenous ACE2 expression in Calu-3 cells**

295 Whether HNF1α, HNF1β and HNF4α controlled the endogenous ACE2 expression in Calu-
296 3 cells was unclear. To address this question, HNF1α, HNF1β and HNF4α were knocked down
297 individually in Calu-3 cells. Dicer-substrate siRNAs (DsiRNA) transfection efficiently reduced the
298 target gene expression by more than 50% (Fig. 7A-7C and S4A). We noticed that knocking down
299 HNF1β, but not HNF1α, suppressed HNF4α mRNA and protein expression in Calu-3 cells.
300 Knocking down HNF4α suppressed HNF1α mRNA but not protein (Fig. 7B and 7C). Regarding
301 endogenous ACE2 expression, we found that knocking down HNF1α and HNF1β, but not HNF4α,
302 significantly suppressed ACE2 protein expression (Fig. 7A-7B and S4A). Interestingly, only
303 knocking down HNF1α led to a significant reduction of ACE2 mRNA expression (Fig. 7C).
304 Knocking down HNF1β suppressed ACE2 protein expression (Fig. 7A-7B, S4A) but not mRNA
305 expression in Calu-3 cells (Fig. 7C). Finally, we found that knocking down either HNF1α or HNF1β
306 significantly suppressed SARS-CoV-2 infection in Calu-3 cells (Fig. 7D). Therefore, HNF1α and

307 HNF1β are required to promote the expression of ACE2 and support SARS-CoV-2 infection in
308 Calu-3 cells.

309 **HNF1-dependent ACE2 expression is suppressed in SAMHD1 KO Calu-3 cells**

310 We hypothesized that the functions of HNF1α and HNF1β in promoting endogenous ACE2
311 expression was suppressed in the SAMHD1 KO Calu-3 cells. To test the hypothesis, transient
312 HNF1α and HNF1β knockdown was performed in SAMHD1 KO cells to examine if the ACE2
313 expression was less dependent on HNF1α and HNF1β when their expression was suppressed
314 upon SAMHD1 deficiency. We found that HNF1α and HNF1β protein expression in KO1 and KO2
315 cells could still be suppressed by DsiRNA knockdown despite their lower expression levels
316 compared to Ctrl cells (Fig. 8A-8C and S4B). Knocking down HNF1α and HNF1β significantly
317 reduced ACE2 protein expression in Ctrl cells (Fig. 8A, 8D and S4B). In the case of KO1 and KO2
318 cells, the suppression of ACE2 protein expression by HNF1α and HNF1β knockdown was
319 mitigated. Knocking down HNF1α, but not HNF1β, reduced ACE2 mRNA expression in Ctrl cells
320 (Fig. 8E). In contrast, HNF1α knockdown was less potent in further suppressing ACE2 mRNA in
321 KO1 and KO2 cells (Fig. 8E). Given that endogenous ACE2 expression was more dependent on
322 HNF1α and HNF1β in Calu-3 Ctrl cells (Fig. 8D and 8E), our data suggest that SAMHD1
323 expression promotes HNF1-dependent ACE2 expression in Calu-3 cells.

324

325 **Discussion**

326 In this study, we investigated the role of SAMHD1 in SARS-CoV-2 infection of Calu-3 cells,
327 which expressed endogenous ACE2 and supported productive viral replication. Similar to our
328 previous study using other cell types [32], SARS-CoV-2 replication was enhanced in SAMHD1
329 expressing Calu-3 cells. Previous study showed that inhibition of IFN signaling by the JAK1/2
330 inhibitor baricitinib alleviated the replication restraint of SARS-CoV-2 in HEK293T cells with
331 SAMHD1 KO [32], while in the current study, baricitinib treatment did not promote SARS-CoV-2
332 replication in SAMHD1 KO Calu-3 cells. We noticed that baricitinib treatment promoted the
333 intracellular viral N RNA and protein levels of SARS-CoV-2 in Calu-3 Ctrl cells but did not change
334 the production of infectious progeny viruses. In contrast, baricitinib treatment enhanced neither
335 the viral RNA nor viral protein levels in SAMHD1 KO1 and KO2 cells, suggesting that some
336 fundamental mechanisms to SARS-CoV-2 replication were disrupted in KO1 and KO2 cells rather
337 than IFN signaling.

338 HEK293T cells support productive replication of SARS-CoV-2 despite negligible expression
339 of ACE2 and TMPRSS2 [80-82]. Through a CRISPR/Cas9 KO library screen, an alternative viral
340 receptor TMEM106B was found to be required for SARS-CoV-2 replication in HEK293T cells [82].
341 In contrast, SARS-CoV-2 infection in Calu-3 cells exhibits a strong dependence on ACE2
342 expression, as evidenced by multiple CRISPR/Cas9 library screens where ACE2 was consistently

343 the most critical host factor identified [71-73]. We found that compared to other known viral entry
344 factors, ACE2 expression was significantly reduced in SAMHD1 KO Calu-3 cells, with consistent
345 results observed in both the KO1 and KO2 lines. SAMHD1 KO significantly hindered SARS-CoV-
346 2 S protein-mediated viral entry in Calu-3 cells; however, once this barrier was bypassed by VSV-
347 G pseudotyping, the single-cycle infection of SARS-CoV-2 replicon was restored. Therefore,
348 SAMHD1 KO abolished ACE2-dependent and S-mediated viral entry which is required for SARS-
349 CoV-2 infection of Calu-3 cells, but not HEK293T cells.

350 We questioned how SAMHD1 promoted ACE2 expression in Calu-3 cells. We found that
351 SAMHD1 KO repressed ACE2 mRNA expression in Calu-3 cells, but ACE2 mRNA stability was
352 unaffected. This suggests that SAMHD1 KO might pre-transcriptionally or transcriptionally
353 suppress ACE2 mRNA expression. We found that SAMHD1 KO suppressed the expression levels
354 of HNF1α and HNF1β, which in turn downregulated the expression of ACE2 and SARS-CoV-2
355 infection. We functionally validated the inhibition of HNF1-mediated endogenous ACE2
356 expression in SAMHD1 KO Calu-3 cells. To the best of our scope, this is the first study functionally
357 confirming the role of HNF1α and HNF1β in promoting ACE2 expression in lung epithelial cells.
358 Interestingly, although HNF1α and HNF1β were previously defined to be transcription factors of
359 ACE2 by binding to the HNF1 response element of the proximal promoter [64, 65], we found that
360 only HNF1α was required for ACE2 mRNA expression in Calu-3 cells. HNF1β was however

361 required for ACE2 protein but not mRNA expression. These findings implied that SAMHD1 KO
362 contributed to suppress ACE2 mRNA and protein levels through downregulation of HNF1α and
363 HNF1β expression, respectively (summarized mechanisms in Fig. 9).

364 It is still in question how SAMHD1 promotes the expression and activity of HNF1α and
365 HNF1β in driving ACE2 expression. SAMHD1 is a nuclear protein that has not been identified to
366 have direct transcriptional function. SAMHD1 mainly interacts with single-stranded RNA or DNA
367 but had low affinity to double-stranded DNA [83, 84]. It is possible that SAMHD1 depletion may
368 have created some cellular stresses that inhibit the expression of HNF1α and HNF1β. We found
369 that SAMHD1 KO Calu-3 cells spontaneously express higher IL-6 than Ctrl cells. Indeed, the
370 expression of several proinflammatory cytokines including IL-1α, IL-1β, CSF2 and IL-11 were also
371 upregulated in both KO1 and KO2 clones (Table S2). Some studies suggest that HNF1α and
372 HNF1β expressions are suppressed upon inflammation. Firstly, the expression of HNF1α in
373 hepatocytes was suppressed through a positive feedback circuit when mice were treated with
374 dimethylnitrosamine that induced liver inflammation followed by hepatic fibrogenesis [85].
375 Secondly, the expression of HNF1β was downregulated by IFN-γ in kidney cells HK-2, while
376 lipopolysaccharide injection downregulated HNF1β expression in mouse kidney cells [86]. Thirdly,
377 we found that HNF4α knockdown reduced HNF1α mRNA expression in Calu-3 cells although the
378 protein change was not observed (Fig. 7A-7C). One recent study suggests HNF4α is

379 transcriptionally suppressed by inflammatory stimuli such as IL-6 and IL-1β in differentiated
380 HepaRG cells [87]. It is possible that the enhanced expression of proinflammatory cytokines of
381 SAMHD1 KO Calu-3 cells suppresses HNF4α expression, thereby decreasing the expression of
382 HNF1α. We also found that HNF1β positively regulated HNF4α expression (Fig. 7B-7C). It is
383 possible that HNF1β plays an upstream role in the expression of HNF1α and HNF4α in Calu-3
384 cells. SAMHD1 expression prevents spontaneous proinflammatory cytokine production mainly
385 through inhibition of NF-kB signaling [25, 28] and preventing RIG-I like receptor signaling and
386 cGAS-STING activation by self-RNA or self-DNA species [17-24]. Therefore, SAMHD1 expression
387 maintains innate immune homeostasis, which sustains the endogenous expressions of HNF1α
388 and HNF1β to support ACE2 expression. Further investigation is needed to confirm the idea.

389 We noticed that several cell surface proteins and proteins related to extracellular matrix
390 distinguished SAMHD1 KO Calu-3 cells from Ctrl cells through the PCA (Fig. S2C). Similarly, gene
391 ontology (GO) enrichment analysis (GOEA) of cellular components to the 681 common DEGs of
392 SAMHD1 KO Calu-3 cells suggest that cell periphery was the best enriched term having the
393 lowest FDR-adjusted P value (Fig. S5 and table S3). Among the top ten GO terms, four terms
394 were correlated with cell surface membranes in addition to cell periphery (including plasma
395 membrane, apical plasma membrane and cell surface) while five terms were correlated with
396 extracellular matrix (including extracellular matrix, external encapsulating structure, extracellular

397 region, extracellular space, collagen-containing extracellular matrix). Although we did not observe
398 any validated SARS-CoV-2 entry factors on the 681 common DEGs except ACE2, TMPRSS2 and
399 furin in which only ACE2 was found to be consistently downregulated in both KO1 and KO2 clones,
400 it might be possible that the changes in cell surface and extracellular matrix structures contribute
401 to the suppressed SARS-CoV-2 infection and viral entry in SAMHD1 KO Calu-3 cells. Any
402 combinatorial effects of the DEGs contributing to the changes in cell surface and extracellular
403 structures that may potentially suppress SARS-CoV-2 infection shall be valuable in future
404 investigation (Table S4).

405 Why SAMHD1 depletion affected the expression of so many genes encoding cell surface
406 and extracellular matrix proteins remains unclear. One study suggests SAMHD1 expression
407 promotes focal adhesion kinase (FAK) signaling by binding to cortactin, and in turn activated Rac
408 family small GTPase 1 (Rac1)-mediated lamellipodia formation in human clear cell renal cell
409 carcinoma [88]. It is possible that SAMHD1 KO Calu-3 had lower activity of FAK and Rac-1.
410 Interestingly, Rac-1 was found to promote SARS-CoV-2 entry via macropinocytosis in ACE2-
411 expressing cells [89]. Thus, SAMHD1 may enhance SARS-CoV-2 infection by macropinocytosis
412 through cortactin, FAK and Rac-1, in addition to promoting HNF1-mediated ACE2 expression.
413 Further investigation is required for the detailed mechanism by which SAMHD1 promotes SARS-
414 CoV-2 infection in physiologically relevant cell types.

415 We were surprised to find that only KO2 but not KO1 clone had spontaneous IFN-I responses
416 (Fig. 1C). Indeed, based on PCA, KO2 cells were clustered away from Ctrl and KO1 cells mainly
417 by several ISGs (Fig. S2C). IFN-I production requires activation of IRF3/7 in addition to NF-κB
418 signal pathway [90]. KO1 cells exhibited complete absence of SAMHD1 protein since expression
419 was abolished with sgRNA1 frameshifting exon 1 at ^{11}Lysine (Fig. 1A, 1B and S1A). KO2 cells
420 may express a truncated protein consisting of the first 1-149 amino acids of SAMHD1. Whether
421 the truncated SAMHD1 protein (aa. 1-149) contributes to IFN-I activation and ISG expression in
422 Calu-3 cells is unclear and will require further investigation.
423 In summary, we found that SAMHD1 is a proviral factor to SARS-CoV-2 infection in Calu-3
424 cells by enhancing S protein-mediated viral entry through maintaining HNF1-mediated ACE2
425 expression. Our study shed light on a novel function and mechanism of SAMHD1 in facilitating
426 SARS-CoV-2 infection in lung epithelial cells.
427

428 **Materials and Methods**

429 **Cell culture**

430 Cell culture was performed as previously described [91, 92]. The original wildtype Calu-3
431 cells were obtained from ATCC (HTB-55™). Wild-type Calu-3 cells as well as Ctrl, KO1 and KO2
432 cells were maintained in DMEM/F12 (ThermoFisher Scientific, Cat. no. 11320033) with 20% FBS,

433 100 U/mL penicillin (Gibco, Cat. no. 15140122), and 100 µg/mL streptomycin (Gibco, Cat. no.
434 15140122). Huh7.5 cells were kindly provided by Dr. Balaji Manicassamy (University of Iowa) [41].
435 Vero-hTMPRSS2 cells were cultured in DMEM (ThermoFisher Scientific, Cat. no. 11965092) with
436 10% FBS, 100 U/mL penicillin, 100 µg/mL streptomycin and 5 µg/mL blasticidin (Gibco, Cat. no.
437 A1113903) as previously described [93]. Huh7.5 cells were cultured in DMEM with 10% FBS, 100
438 U/mL penicillin, 100 µg/mL streptomycin. Actinomycin D (SellekChemicals, Cat. no. S8964),
439 remdesivir (MCE, Cat. no.: HY-104077) and baricitinib (MCE, Cat. no.: HY-15315) were dissolved
440 in dimethyl sulfoxide (DMSO) and stored at -20°C.

441 **Generation of SAMHD1 KO Calu-3 cells**

442 SAMHD1 KO Calu-3 cells were generated similarly as previously described with some
443 modifications [91, 92]. Briefly, third generation lentiviral particles were rescued from HEK293T
444 cells (1 x 10^7) transfected with lentiCRISPR v2-puro empty vector, lentiCRISPR v2-puro-sgRNA1,
445 or lentiCRISPR v2-puro-sgRNA2 together with psPAX2, and pMD2.G (ratio 4:3:1) by PEI (1:5
446 ratio). The target sequence of sgRNA 1 guided SpCas9 cutting at exon 1 of SAMHD1 gene (chr20:
447 36,951,611/36,951,612) while that of sgRNA 2 targeted SpCas9 for exon 4 (chr20:
448 36,935,087/36,935,088). The template sequence for sgRNA1 was *5'-*
449 *GTCATCGCAACGGGGACGCTTGG* and sgRNA2 was *5'-CTTCGATACATCAAACAGCTGGG*.
450 At 24 hrs post-transfection (hpt), the culture supernatant was replenished with fresh media. At 72

451 hpt, the 12 mL culture supernatant was cleared by 500 x g 5 min centrifugation followed with 0.45
452 μm filtering and concentrated by lenti-concentrator (ORIGENE, Cat. no TR30026) into 1mL media.
453 A day before transduction, 4 x 10^5 Calu-3 cells were seeded in 12 well plates. On the day of
454 transduction, the culture supernatant of the Calu-3 cells was replaced with the 1mL concentrated
455 virus. At 24 hpi, the culture supernatant was replaced with fresh DMEM/F12 with 20% FBS, 100
456 U/mL penicillin, and 100 μg/mL streptomycin. At 72 hpi, cells were selected against 1 μg/mL
457 puromycin. The survival cells of the transduced populations were purified by limited dilution on a
458 96 well plate. Finally, the purified cell clones were verified for expression of SAMHD1 and
459 genotyping.

460 **RNA interference and transfection**

461 DsiRNAs were oligo-duplex and the sequences were predesigned by Integrated DNA
462 Technologies (IDT) [94]. Cells were transfected with DsiRNA with Lipofectamine RNAiMAX
463 Reagent (ThermoFisher Scientific, Cat. no. 13778150). In brief, equal volume of OPTIMEM-
464 (Gibco, Cat. no. 31985070) diluted DsiRNA (150 μl for 24 well format and 300 μl for 12 well format)
465 and OPTIMEM-diluted lipofectamine RNAiMAX (1:3 ratio) were mixed and incubated for 20 min
466 at room temperature. Cell suspension (0.5 mL in 24 well format and 1 mL in 12 well format) was
467 mixed with the 600 μl DsiRNA/lipofectamine RNAiMax complex. At 24 hpt, culture supernatant
468 was replaced with fresh medium. Cells were harvested at indicated time points. The DsiRNA

469 sequences used in the current study were listed in Table S5.

470 **Virus stocks**

471 Authentic SARS-CoV-2 (Wuhan-Hu-1) was rescued from Vero-hTMPRSS2 transfected with
472 bacterial artificial chromosome carrying SARS-CoV-2 genome (BAC-SARS-CoV-2) as previously
473 described with some modifications [95]. In brief, 1 x 10^7 Vero-hTMPRSS2 cells were seeded in a
474 T75 flask a day before transfection without blasticidin. Vero-hTMPRSS2 cells were transfected
475 with 10 μg BAC-SARS-CoV-2 with lipofectamine 3000 (ThermoFisher Scientific, Cat. no.
476 L3000008). At 24 hpi, the culture supernatant was replaced with serum-free DMEM. At 72 hpi,
477 80% cytopathic effect was observed. The crude culture supernatant was collected for one freeze-
478 thaw cycle. Then, the supernatant was cleared by pelleting debris at 2,000 x g, 10 min, 4°C. The
479 viral containing supernatant was aliquoted and frozen at -80°C for subsequent studies.

480 ΔS-VRP(G) was rescued from Huh7.5 transfected with BAC carrying spike-defective SARS-
481 CoV-2 genome (BAC-ΔS-Gluc-T2A-nGFP) together with VSV-G expression plasmid similarly as
482 previously described [41, 96].

483 HIV-1-spike-Luc/ZsGreen (BEI resources, Cat. no. NR-53818) was a generous gift donated
484 by Dr. Jesse Bloom (Fred Hutchinson Cancer Center) and Dr. Alejandro Benjamin Balazs
485 (Harvard University) and available on BEI resources. The titration of the stock batch (Lot:
486 70042784) was 4.99 × 10^5 relative luciferase tissue culture infectious dose 50% ($TCID_{50}$) units in

487 HEK293-hACE2 cells at 48 hpi.

488 **Virus infection assays**

489 For authentic SARS-CoV-2, cells were seeded a day prior to infection. The culture
490 supernatant was replaced with serum free DMEM prior to infection. Then, the cells were incubated
491 with SARS-CoV-2 at appropriate MOI for 1 hr. Then, the virus inoculum was aspirated. The cells
492 were washed twice with DPBS (Gibco, Cat. no. 14190144). Then, cells were replenished with
493 serum free DMEM. The culture supernatants or infected cells were harvested at indicated time
494 points.

495 For ΔS-VRP(G), cells were infected as previously described [41, 96] and similarly as that of
496 the authentic SARS-CoV-2 but with 2 hr virus inoculation instead of 1 hr. After virus inoculation,
497 infected cells were washed twice with DPBS. Cells were then replenished with DMEM/F12 with
498 20% FBS, 100 U/mL penicillin, and 100 μg/mL streptomycin. The culture supernatants or infected
499 cells were harvested at indicated time points.

500 For HIV-1-spike-Luc/ZsGreen, cells were infected as previously described [43, 44]. Cells
501 were incubated with the virus in the presence of 5 μg/ml polybrene for 1 hr in DMEM/F12 with
502 20% FBS, 100 U/mL penicillin, and 100 μg/mL streptomycin. Then, virus inoculum was removed.
503 Fresh DMEM/F12 with 20% FBS, 100 U/mL penicillin, and 100 μg/mL streptomycin was added.
504 At 48 hpi, infected cells were harvested for downstream analysis.

505 **Plaque assay**

506 A day before infection, 4 x 10^5 or 8 x 10^5 Vero-hTMPRSS2 cells were seeded respectively
507 on 12- or 6- well plates. Vero-hTMPRSS2 cells were infected with serially diluted viral stocks for
508 1 hr. Then, the virus inoculum was removed. Infected cells were overlayed with 1% agarose in
509 DMEM/ DPBS (1:1). At 72 hpi, infected cells were overnight fixed with 4% paraformaldehyde/PBS
510 (ThermoFisher Scientific, Cat. no. J19943.K2). Then, the overlay was removed, and the cells were
511 stained with 0.5% crystal violet in 10% methanol for at least 5 min. Plaques were visualized. Virus
512 concentration was calculated based on the number of plaques in the countable dilution.

513 **Viral copy number detection**

514 Viral RNA was extracted by RNeasy Plus kit (QIAGEN, Cat. no. 74134) in which viral
515 containing solutions and RLT plus lysis buffer was in 1:4 ratio. Viruses were lysed in RLT plus
516 lysis buffer for 10 min at room temperature. The purified viral RNA was reverse transcribed using
517 the iScript cDNA Synthesis Kit (BIO-RAD, Cat. no. 1708891). Viral RNA was detected by the
518 qPCR primer pair targeting the viral RdRP (Table S5) with iTaq™ Universal SYBR® Green
519 Supermix (BIO-RAD, Cat. no.1725124) [97, 98]. Standard curve for the number of single stranded
520 DNA against Ct value was generated using the BAC-SARS-CoV-2 DNA. The copy number of
521 single stranded RNA was estimated from the copy number of cDNA in each sample.

522 **Genomic DNA sequencing**

523 The genome DNA of Ctrl, KO1 and KO2 cells were purified with DNeasy Blood and Tissue
524 Kits for DNA Isolation (QIAGEN, Cat. no. 69504). Exon 1 and exon 4 regions encompassing the
525 Cas9 cleavage sites were amplified by Phusion High-Fidelity DNA Polymerase (NEB, Cat. no.
526 M0530L). The sequences of the PCR primer pair for amplifying exon 1 was *5'-*
527 *CGAAGGGCTCAACTGTCAGT* (forward) and *5'-CTCGGGTCTTCCTTTCCTCG* (reverse) and
528 that of exon 4 was *5'-TGATCTGTCTGGTAGTGATACCT* (forward) and *5'-*
529 *CGATTGTGTGAAGCTCCTGG* (reverse). Then, the PCR products were submitted for sanger
530 sequencing services provided by Genomics Division of Iowa Institute of Human Genetics
531 (University of Iowa) using the forward primers.

532 **Cellular dATP detection**

533 Cellular dATP levels were measured by a single nucleotide RT incorporation assay
534 previously described [37, 40, 92]. In brief, 2 x 10^6 cells were harvested for dNTP extraction with
535 50% methanol. Methanol extract was dried at 80°C for 1 hr and then reconstituted in reaction
536 buffer at appropriate dilution within linear range of the assay as previously described for dATP
537 levels detection. The levels of cellular dATP were calculated by extrapolating the relative band
538 intensity to the standard curve created by the parallel reactions.

539 **Western blot analysis**

540 Upon harvest, cells were washed once with DPBS and lysed with 1 x cell lysis buffer (Cell

541 Signaling Technology, Cat. no. 9803) with phosphatase and protease inhibitor (ThermoFisher
542 Scientific, Cat. no. A32961) for 10 to 30 min until complete lysis. Cell debris was removed by
543 centrifugation at 16.1 kg for 10 min at 4°C. Total protein concentration was estimated by Pierce™
544 BCA Protein Assay Kit (ThermoFisher Scientific, Cat. no. 23225). Protein samples with normalized
545 total protein levels were mixed with 5 x protein sample buffer (0.25 M Tris-Cl pH 6.8, 20% glycerol,
546 10% SDS and 1% saturated bromophenol blue) to the final concentration of 1 x and heat-
547 denatured at 98°C for 10 min. Cellular protein (10 to 25 μg) was loaded onto polyacrylamide gels
548 for Western blot analysis as previous described [91]. Primary antibodies used were as follows:
549 Anti-GAPDH (BIORAD, Cat. no. AHP1628), anti-viral N (BEI resources, Cat. no. NR-56223), anti-
550 viral S (ThermoFisher Scientific, Cat. no. PA5114451), anti-SAMHD1 (Abcam, Cat. no. ab117908),
551 anti-STAT1 (Cell Signaling Technology, Cat. no. 9172T), anti-p-STAT1 (Cell Signaling Technology,
552 Cat. no. 8826T), anti-ACE2 (Cell Signaling Technology, Cat. no. 92485T), anti-TMPRSS2 (Santa
553 Cruz Biotechnology, Cat. no. sc-515727), anti-HNF1α (Cell Signaling Technology, Cat. no.
554 89670T), anti-HNF1β (Proteintech, Cat no. 12533-1-AP) and anti-HNF4α (Cell Signaling
555 Technology, Cat. no.3113T). For secondary antibody, goat anti-mouse IgG (H+L) HRP (Promega,
556 Cat. no. W4021) or goat anti-rabbit IgG (H+L) HRP (Promega, W401B) was used. Immunoblots
557 were developed with Odyssey Fc Imager. Protein band intensity was quantified by Image Studio™.

558 **RNA extraction and RT-qPCR**

559 Cellular RNA extraction was performed with RNeasy Plus Kits according to the
560 manufacturer's instructions. Upon harvest, cells were washed once with DPBS and lysed with
561 RLT plus lysis buffer. After column purification, 1 μg of purified RNA was used for reverse
562 transcription through iScript cDNA Synthesis Kit. The cDNA product was used for qPCR
563 quantification with iTaq Universal SYBR Green supermix. SYBR signal was quantified by
564 QuantStudio™ 3 Real-Time PCR or CFX Duet Real-Time PCR System. The qPCR primer pairs
565 were either previously designed (including Viral E [99], 18S RNA [100] , IL-6 [25], OAS1 [101],
566 ACE2 and dACE2 [55]), predesigned by PrimerBank [102] or designed in-house based on NCBI
567 primer-BLAST with Primer3 adjustment (Table S5).

568 **Luciferase detection**

569 To detect secreted *Guassia* luciferease activity, 20 μl of culture supernatant was incubated
570 with 50 μl of the working solution of Pierce™ Gaussia Luciferase Flash Assay Kit (ThermoFisher
571 Scientific, Cat. no. 16158) for quantification of the resulting chemiluminescence following
572 manufacturer's instruction. To detect cellular firefly luciferase 2 activity, cells were washed once
573 with DPBS and lysed in 1 x passive lysis buffer (Promega, Cat. no. E1941) supplemented with
574 phosphatase and protease inhibitor. At 30 min lysis, cell debris were removed by centrifugation at
575 16.1 kg for 10 min at 4°C. Total protein concentration was estimated by Pierce™ BCA Protein
576 Assay Kit. 10 μl of the PLB lysate was incubated with 100 μl of LAR-II substrate reagent of the

577 Dual-Luciferase® Reporter Assay System following manufacturer's instruction to quantify the
578 resulting chemiluminescence (Promega, Cat. no. E1980). The cellular firefly luciferase 2 activities
579 were calculated as follow: ($RLU_{infected}$ per one microgram protein) – ($RLU_{uninfected}$ per one
580 microgram protein).

581 **mRNA-sequencing**

582 Calu-3 Ctrl, KO1 and KO2 cells (8 x 10^5) were seeded in 6 well plates in biological triplicate.
583 Cells were cultured in 2 mL DMEM/F12 with 20% FBS, 100 U/mL penicillin, and 100 µg/mL
584 streptomycin. At 20 hrs after seeding, cells were washed once with DPBS and lysed with RLT plus
585 lysis buffer. Cellular RNA was purified with RNeasy Plus kit following manufacturer's instructions.
586 All RNA samples got RNA integrity Number (RIN) scores equal to or more than 9.9 as determined
587 by Agilent BioAnalyzer by Genomics Division of Iowa Institute of Human Genetics (University of
588 Iowa). The subsequent steps of the mRNA-Seq were performed by the Genomics Division using
589 manufacturer recommended protocols. Briefly, at least 500 ng of DNase I-treated total RNA was
590 used to prepare sequencing libraries using the Illumina stranded mRNA library preparation kit
591 (Illumina, Cat. no. 20040534). Barcoded libraries were quantified using a Qubit fluorometer
592 (ThermoFisher Scientific) and pooled together to give the same molar concentration per sample.
593 The pooled libraries were sequenced on the Element AVITI24 sequencing platform on a
594 Cloudbreak FS 150 cycle (2 x 75 bp) medium output sequencing flow cell (Element Biosciences,

595 Cat. no. 860-00014) to generate at least 30M paired-end sequencing reads per sample. The raw
596 base files were converted to FASTQ files using the Bases2fastq v2.1 tool. The mRNA-seq data
597 have been deposited in the Gene Expression Omnibus (GEO) and an accession number will be
598 obtained.

599 **Bioinformatic analysis for mRNA-sequencing**

600 The bioinformatic analysis to the raw FASTQ data obtained from mRNA-sequencing was
601 performed by Bioinformatics Division, Iowa Institute of Human Genetics (University of Iowa). In
602 brief, PCA including PCA plot, PCA biplot and DEG analysis were generated by SALMON DeSeq2.
603 Pathway analysis including GOEA was performed by iPathwayGuide platform (ADVAITABIO).

604 **Statistical analysis**

605 At least biological triplicate was performed for each experiment throughout the study.
606 Statistical analysis was performed by GraphPad Prism. For the dataset of the mRNA-seq
607 experiment, FDR-adjusted P value was obtained. Only changes that had P values less than 0.05
608 were considered statistically significant.

609

610 **Acknowledgements**

611 We thank Drs. Balaji Manicassamy and Patrick Sinn for their invaluable support during this
612 study. We thank Drs. Jesse Bloom and Alejandro Benjamin Balazs for the resources donated to

613 Biodefense and Emerging Infections Research Resources Repository (BEI Resources). The
614 following reagents were obtained through BEI Resources, NIAID, NIH: (1) SARS-Related
615 Coronavirus 2, Wuhan-Hu-1 Spike-Pseudotyped Lentivirus, Luc2/ZsGreen, NR-53818 and (2)
616 Monoclonal Anti-SARS-Related Coronavirus 2 Nucleocapsid Protein (produced in vitro), NR-
617 56223. The mRNA seq data herein were obtained at the Genomics Division (RRID: SCR_023422)
618 and the Bioinformatics Division of the Iowa Institute of Human Genetics which are supported, in
619 part, by the University of Iowa Carver College of Medicine. We also thank Mr. Fernando William
620 Moreira Santana for technical assistance. We appreciate valuable discussions with the members
621 of Dr. Wu's, Dr. Perlman's, and Dr. Sinn's laboratories at the University of Iowa as well as Dr.
622 Constanza Espada from the University of Missouri.

623

624 **Author Contributions**

625 Conceptualization: Pak Hin Hinson Cheung, Li Wu.

626 Data curation: Pak Hin Hinson Cheung, Shravya Honne.

627 Formal analysis: Pak Hin Hinson Cheung, Shravya Honne.

628 Funding acquisition: Li Wu, Baek Kim, Stanley Perlman.

629 Investigation: Pak Hin Hinson Cheung, Shravya Honne.

630 Methodology: Pak Hin Hinson Cheung, Pearl Chan, Hua Yang, Baek Kim, Li Wu.

Project administration: Li Wu, Baek Kim.

Resources: Li Wu, Pearl Chan, Baek Kim, Stanley Perlman.

Supervision: Li Wu, Baek Kim, Stanley Perlman.

Writing – original draft: Pak Hin Hinson Cheung, Li Wu.

Writing – review & editing: Pak Hin Hinson Cheung, Hua Yang, Pearl Chan, Li Wu.

Funding

This work was supported in part by National Institutes of Health grants R21AI181742 (to L.W.), R01AI129269 (to S.P.), and R01AI136581 and R01AI162633 (to B.K.). L.W. is also supported by the NIH grants R01AI189220, R33AI169659, and P30CA086862-25S1. The funders had no role in study design, data collection and analysis, decision to publish, or preparation of the manuscript.

References

1. Hrecka K, Hao C, Gierszewska M, Swanson SK, Kesik-Brodacka M, Srivastava S, et al. Vpx relieves inhibition of HIV-1 infection of macrophages mediated by the SAMHD1 protein. Nature. 2011;474(7353):658-61. Epub 20110629. doi: 10.1038/nature10195. PubMed PMID: 21720370; PubMed Central PMCID: PMCPMC3179858.

2. Laguette N, Sobhian B, Casartelli N, Ringeard M, Chable-Bessia C, Ségéral E, et al. SAMHD1 is the dendritic- and myeloid-cell-specific HIV-1 restriction factor counteracted by Vpx. Nature. 2011;474(7353):654-7. Epub 20110525. doi: 10.1038/nature10117. PubMed PMID: 21613998; PubMed Central PMCID: PMCPMC3595993.

652 3. Baldauf HM, Pan X, Erikson E, Schmidt S, Daddacha W, Burggraf M, et al. SAMHD1 restricts
653 HIV-1 infection in resting CD4(+) T cells. Nat Med. 2012;18(11):1682-7. doi: 10.1038/nm.2964.
654 PubMed PMID: 22972397; PubMed Central PMCID: PMCPMC3828732.

655 4. Sze A, Belgnaoui SM, Olagnier D, Lin R, Hiscott J, van Grevenynghe J. Host restriction factor
656 SAMHD1 limits human T cell leukemia virus type 1 infection of monocytes via STING-mediated
657 apoptosis. Cell Host Microbe. 2013;14(4):422-34. doi: 10.1016/j.chom.2013.09.009. PubMed
658 PMID: 24139400.

659 5. Sommer AF, Rivière L, Qu B, Schott K, Riess M, Ni Y, et al. Restrictive influence of SAMHD1
660 on Hepatitis B Virus life cycle. Sci Rep. 2016;6:26616. Epub 20160527. doi: 10.1038/srep26616.
661 PubMed PMID: 27229711; PubMed Central PMCID: PMCPMC4882586.

662 6. Businger R, Deutschmann J, Gruska I, Milbradt J, Wiebusch L, Gramberg T, et al. Human
663 cytomegalovirus overcomes SAMHD1 restriction in macrophages via pUL97. Nat Microbiol.
664 2019;4(12):2260-72. Epub 20190923. doi: 10.1038/s41564-019-0557-8. PubMed PMID:
665 31548682.

666 7. Zhang K, Lv DW, Li R. Conserved Herpesvirus Protein Kinases Target SAMHD1 to Facilitate
667 Virus Replication. Cell Rep. 2019;28(2):449-59.e5. doi: 10.1016/j.celrep.2019.04.020. PubMed
668 PMID: 31291580; PubMed Central PMCID: PMCPMC6668718.

669 8. Kim ET, White TE, Brandariz-Núñez A, Diaz-Griffero F, Weitzman MD. SAMHD1 restricts
670 herpes simplex virus 1 in macrophages by limiting DNA replication. J Virol. 2013;87(23):12949-
671 56. Epub 20130925. doi: 10.1128/jvi.02291-13. PubMed PMID: 24067963; PubMed Central
672 PMCID: PMCPMC3838123.

673 9. Sliva K, Martin J, von Rhein C, Herrmann T, Weyrich A, Toda M, et al. Interference with
674 SAMHD1 Restores Late Gene Expression of Modified Vaccinia Virus Ankara in Human Dendritic
675 Cells and Abrogates Type I Interferon Expression. J Virol. 2019;93(22). Epub 20191029. doi:
676 10.1128/jvi.01097-19. PubMed PMID: 31462561; PubMed Central PMCID: PMCPMC6819912.

677 10. James CD, Youssef A, Prabhakar AT, Otoa R, Roe JD, Witt A, et al. Human papillomavirus
678 16 replication converts SAMHD1 into a homologous recombination factor and promotes its
679 recruitment to replicating viral DNA. J Virol. 2024;98(9):e0082624. Epub 20240828. doi:
680 10.1128/jvi.00826-24. PubMed PMID: 39194246; PubMed Central PMCID: PMCPMC11406955.

681 11. Zhao Z, Han S, Zhang Q, Wang Y, Yue K, Abbas S, et al. Impaired influenza A virus

682 replication by the host restriction factor SAMHD1 which inhibited by PA-mediated
683 dephosphorylation of the host transcription factor IRF3. Virol J. 2024;21(1):33. Epub 20240129.
684 doi: 10.1186/s12985-024-02295-0. PubMed PMID: 38287375; PubMed Central PMCID:
685 PMCPMC10826253.

686 12. Zhao Z, Li Z, Huan C, Liu X, Zhang W. SAMHD1 Inhibits Multiple Enteroviruses by Interfering
687 with the Interaction between VP1 and VP2 Proteins. J Virol. 2021;95(13):e0062021. Epub
688 20210610. doi: 10.1128/jvi.00620-21. PubMed PMID: 33883225; PubMed Central PMCID:
689 PMCPMC8316000.

690 13. An N, Ge Q, Shao H, Li Q, Guo F, Liang C, et al. Interferon-inducible SAMHD1 restricts viral
691 replication through downregulation of lipid synthesis. Front Immunol. 2022;13:1007718. Epub
692 20221130. doi: 10.3389/fimmu.2022.1007718. PubMed PMID: 36532074; PubMed Central
693 PMCID: PMCPMC9755837.

694 14. Cheung PH, Yang H, Wu L. dNTP depletion and beyond: the multifaceted nature of
695 SAMHD1-mediated viral restriction. J Virol. 2025;99(5):e0030225. Epub 20250425. doi:
696 10.1128/jvi.00302-25. PubMed PMID: 40277359; PubMed Central PMCID: PMCPMC12090746.

697 15. Chen S, Bonifati S, Qin Z, St Gelais C, Wu L. SAMHD1 Suppression of Antiviral Immune
698 Responses. Trends Microbiol. 2019;27(3):254-67. Epub 20181015. doi:
699 10.1016/j.tim.2018.09.009. PubMed PMID: 30336972; PubMed Central PMCID:
700 PMCPMC6377309.

701 16. White TE, Brandariz-Nuñez A, Martinez-Lopez A, Knowlton C, Lenzi G, Kim B, et al. A
702 SAMHD1 mutation associated with Aicardi-Goutières syndrome uncouples the ability of SAMHD1
703 to restrict HIV-1 from its ability to downmodulate type I interferon in humans. Hum Mutat.
704 2017;38(6):658-68. Epub 20170502. doi: 10.1002/humu.23201. PubMed PMID: 28229507;
705 PubMed Central PMCID: PMCPMC5738905.

706 17. Coquel F, Silva MJ, Técher H, Zadorozhny K, Sharma S, Nieminuszczy J, et al. SAMHD1
707 acts at stalled replication forks to prevent interferon induction. Nature. 2018;557(7703):57-61.
708 Epub 20180418. doi: 10.1038/s41586-018-0050-1. PubMed PMID: 29670289.

709 18. Maharana S, Kretschmer S, Hunger S, Yan X, Kuster D, Traikov S, et al. SAMHD1 controls
710 innate immunity by regulating condensation of immunogenic self RNA. Mol Cell.
711 2022;82(19):3712-28.e10. Epub 20220922. doi: 10.1016/j.molcel.2022.08.031. PubMed PMID:
712 36150385.

713 19. Rabinowitz J, Vila IK, Luchsinger C, Bertelli C, Schüssler M, Taffoni C, et al. The ability of
714 SAMHD1-deficient monocytes to trigger the Type I IFN response depends on cGAS and
715 mitochondrial DNA. J Biol Chem. 2025;301(8):110430. Epub 20250626. doi:
716 10.1016/j.jbc.2025.110430. PubMed PMID: 40581121; PubMed Central PMCID:
717 PMCPMC12312027.

718 20. Schumann T, Ramon SC, Schubert N, Mayo MA, Hega M, Maser KI, et al. Deficiency for
719 SAMHD1 activates MDA5 in a cGAS/STING-dependent manner. J Exp Med. 2023;220(1). Epub
720 20221108. doi: 10.1084/jem.20220829. PubMed PMID: 36346347; PubMed Central PMCID:
721 PMCPMC9648672.

722 21. Maelfait J, Bridgeman A, Benlahrech A, Cursi C, Rehwinkel J. Restriction by SAMHD1 Limits
723 cGAS/STING-Dependent Innate and Adaptive Immune Responses to HIV-1. Cell Rep.
724 2016;16(6):1492-501. Epub 20160728. doi: 10.1016/j.celrep.2016.07.002. PubMed PMID:
725 27477283; PubMed Central PMCID: PMCPMC4978700.

726 22. Rehwinkel J, Maelfait J, Bridgeman A, Rigby R, Hayward B, Liberatore RA, et al. SAMHD1-
727 dependent retroviral control and escape in mice. Embo j. 2013;32(18):2454-62. Epub 20130719.
728 doi: 10.1038/emboj.2013.163. PubMed PMID: 23872947; PubMed Central PMCID:
729 PMCPMC3770946.

730 23. Behrendt R, Schumann T, Gerbaulet A, Nguyen LA, Schubert N, Alexopoulou D, et al. Mouse
731 SAMHD1 has antiretroviral activity and suppresses a spontaneous cell-intrinsic antiviral response.
732 Cell Rep. 2013;4(4):689-96. Epub 20130822. doi: 10.1016/j.celrep.2013.07.037. PubMed PMID:
733 23972988; PubMed Central PMCID: PMCPMC4807655.

734 24. Oh C, Ryoo J, Park K, Kim B, Daly MB, Cho D, et al. A central role for PI3K-AKT signaling
735 pathway in linking SAMHD1-deficiency to the type I interferon signature. Sci Rep. 2018;8(1):84.
736 Epub 20180108. doi: 10.1038/s41598-017-18308-8. PubMed PMID: 29311560; PubMed Central
737 PMCID: PMCPMC5758801.

738 25. Chen S, Bonifati S, Qin Z, St Gelais C, Kodigepalli KM, Barrett BS, et al. SAMHD1
739 suppresses innate immune responses to viral infections and inflammatory stimuli by inhibiting the
740 NF-κB and interferon pathways. Proc Natl Acad Sci U S A. 2018;115(16):E3798-e807. Epub
741 20180402. doi: 10.1073/pnas.1801213115. PubMed PMID: 29610295; PubMed Central PMCID:
742 PMCPMC5910870.

743 26. Xu B, Sui Q, Hu H, Hu X, Zhou X, Qian C, et al. SAMHD1 Attenuates Acute Inflammation by

744 Maintaining Mitochondrial Function in Macrophages via Interaction with VDAC1. Int J Mol Sci.
745 2023;24(9). Epub 20230426. doi: 10.3390/ijms24097888. PubMed PMID: 37175593; PubMed
746 Central PMCID: PMCPMC10177872.

747 27. Espada CE, Sari L, Cahill MP, Yang H, Phillips S, Martinez N, et al. SAMHD1 impairs type I
748 interferon induction through the MAVS, IKKε, and IRF7 signaling axis during viral infection. J Biol
749 Chem. 2023;299(7):104925. Epub 20230614. doi: 10.1016/j.jbc.2023.104925. PubMed PMID:
750 37328105; PubMed Central PMCID: PMCPMC10404699.

751 28. Yang H, Espada CE, Phillips S, Martinez N, Kenney AD, Yount JS, et al. The host antiviral
752 protein SAMHD1 suppresses NF-κB activation by interacting with the IKK complex during
753 inflammatory responses and viral infection. J Biol Chem. 2023;299(6):104750. Epub 20230424.
754 doi: 10.1016/j.jbc.2023.104750. PubMed PMID: 37100289; PubMed Central PMCID:
755 PMCPMC10318468.

756 29. Programme WHE. Number of COVID-19 deaths reported to WHO (cumulative total): World
757 Health Organisation; 2025. Available from: https://data.who.int/dashboards/covid19/deaths.

758 30. Williams BA, Jones CH, Welch V, True JM. Outlook of pandemic preparedness in a post-
759 COVID-19 world. NPJ Vaccines. 2023;8(1):178. Epub 20231120. doi: 10.1038/s41541-023-
760 00773-0. PubMed PMID: 37985781; PubMed Central PMCID: PMCPMC10662147.

761 31. Sievers BL, Cheng MTK, Csiba K, Meng B, Gupta RK. SARS-CoV-2 and innate immunity:
762 the good, the bad, and the "goldilocks". Cell Mol Immunol. 2024;21(2):171-83. Epub 20231120.
763 doi: 10.1038/s41423-023-01104-y. PubMed PMID: 37985854; PubMed Central PMCID:
764 PMCPMC10805730.

765 32. Oo A, Zandi K, Shepard C, Bassit LC, Musall K, Goh SL, et al. Elimination of Aicardi-
766 Goutières syndrome protein SAMHD1 activates cellular innate immunity and suppresses SARS-
767 CoV-2 replication. J Biol Chem. 2022;298(3):101635. Epub 20220125. doi:
768 10.1016/j.jbc.2022.101635. PubMed PMID: 35085552; PubMed Central PMCID:
769 PMCPMC8786443.

770 33. Ahn JH, Kim J, Hong SP, Choi SY, Yang MJ, Ju YS, et al. Nasal ciliated cells are primary
771 targets for SARS-CoV-2 replication in the early stage of COVID-19. J Clin Invest. 2021;131(13).
772 doi: 10.1172/jci148517. PubMed PMID: 34003804; PubMed Central PMCID: PMCPMC8245175.

773 34. Hui KPY, Ho JCW, Cheung MC, Ng KC, Ching RHH, Lai KL, et al. SARS-CoV-2 Omicron

774 variant replication in human bronchus and lung ex vivo. Nature. 2022;603(7902):715-20. Epub
775 20220201. doi: 10.1038/s41586-022-04479-6. PubMed PMID: 35104836.

776 35. Sanjana NE, Shalem O, Zhang F. Improved vectors and genome-wide libraries for CRISPR
777 screening. Nat Methods. 2014;11(8):783-4. doi: 10.1038/nmeth.3047. PubMed PMID: 25075903;
778 PubMed Central PMCID: PMCPMC4486245.

779 36. Labun K, Montague TG, Krause M, Torres Cleuren YN, Tjeldnes H, Valen E. CHOPCHOP
780 v3: expanding the CRISPR web toolbox beyond genome editing. Nucleic Acids Res.
781 2019;47(W1):W171-w4. doi: 10.1093/nar/gkz365. PubMed PMID: 31106371; PubMed Central
782 PMCID: PMCPMC6602426.

783 37. Diamond TL, Roshal M, Jamburuthugoda VK, Reynolds HM, Merriam AR, Lee KY, et al.
784 Macrophage tropism of HIV-1 depends on efficient cellular dNTP utilization by reverse
785 transcriptase. J Biol Chem. 2004;279(49):51545-53. Epub 20040926. doi:
786 10.1074/jbc.M408573200. PubMed PMID: 15452123; PubMed Central PMCID:
787 PMCPMC1351161.

788 38. Martinez-Lopez A, Martin-Fernandez M, Buta S, Kim B, Bogunovic D, Diaz-Griffero F.
789 SAMHD1 deficient human monocytes autonomously trigger type I interferon. Mol Immunol.
790 2018;101:450-60. Epub 20180809. doi: 10.1016/j.molimm.2018.08.005. PubMed PMID:
791 30099227; PubMed Central PMCID: PMCPMC6258080.

792 39. Espada CE, St Gelais C, Bonifati S, Maksimova VV, Cahill MP, Kim SH, et al. TRAF6 and
793 TAK1 Contribute to SAMHD1-Mediated Negative Regulation of NF-κB Signaling. J Virol.
794 2021;95(3). Epub 20210113. doi: 10.1128/jvi.01970-20. PubMed PMID: 33177202; PubMed
795 Central PMCID: PMCPMC7925110.

796 40. Qin Z, Bonifati S, St Gelais C, Li TW, Kim SH, Antonucci JM, et al. The dNTPase activity of
797 SAMHD1 is important for its suppression of innate immune responses in differentiated monocytic
798 cells. J Biol Chem. 2020;295(6):1575-86. Epub 20191230. doi: 10.1074/jbc.RA119.010360.
799 PubMed PMID: 31914403; PubMed Central PMCID: PMCPMC7008377.

800 41. Malicoat J, Manivasagam S, Zuñiga S, Sola I, McCabe D, Rong L, et al. Development of a
801 Single-Cycle Infectious SARS-CoV-2 Virus Replicon Particle System for Use in Biosafety Level 2
802 Laboratories. J Virol. 2022;96(3):e0183721. Epub 20211201. doi: 10.1128/jvi.01837-21. PubMed
803 PMID: 34851142; PubMed Central PMCID: PMCPMC8826801.

42. Kokic G, Hillen HS, Tegunov D, Dienemann C, Seitz F, Schmitzova J, et al. Mechanism of SARS-CoV-2 polymerase stalling by remdesivir. Nat Commun. 2021;12(1):279. Epub 20210112. doi: 10.1038/s41467-020-20542-0. PubMed PMID: 33436624; PubMed Central PMCID: PMCPMC7804290.

43. Crawford KHD, Eguia R, Dingens AS, Loes AN, Malone KD, Wolf CR, et al. Protocol and Reagents for Pseudotyping Lentiviral Particles with SARS-CoV-2 Spike Protein for Neutralization Assays. Viruses. 2020;12(5). Epub 20200506. doi: 10.3390/v12050513. PubMed PMID: 32384820; PubMed Central PMCID: PMCPMC7291041.

44. Crawford KHD, Dingens AS, Eguia R, Wolf CR, Wilcox N, Logue JK, et al. Dynamics of Neutralizing Antibody Titers in the Months After Severe Acute Respiratory Syndrome Coronavirus 2 Infection. J Infect Dis. 2021;223(2):197-205. doi: 10.1093/infdis/jiaa618. PubMed PMID: 33535236; PubMed Central PMCID: PMCPMC7543487.

45. Baggen J, Jacquemyn M, Persoons L, Vanstreels E, Pye VE, Wrobel AG, et al. TMEM106B is a receptor mediating ACE2-independent SARS-CoV-2 cell entry. Cell. 2023;186(16):3427-42.e22. Epub 20230707. doi: 10.1016/j.cell.2023.06.005. PubMed PMID: 37421949; PubMed Central PMCID: PMCPMC10409496.

46. Liao Z, Wang C, Tang X, Yang M, Duan Z, Liu L, et al. Human transferrin receptor can mediate SARS-CoV-2 infection. Proc Natl Acad Sci U S A. 2024;121(10):e2317026121. Epub 20240226. doi: 10.1073/pnas.2317026121. PubMed PMID: 38408250; PubMed Central PMCID: PMCPMC10927525.

47. Wang K, Chen W, Zhang Z, Deng Y, Lian JQ, Du P, et al. CD147-spike protein is a novel route for SARS-CoV-2 infection to host cells. Signal Transduct Target Ther. 2020;5(1):283. Epub 20201204. doi: 10.1038/s41392-020-00426-x. PubMed PMID: 33277466; PubMed Central PMCID: PMCPMC7714896.

48. Wang S, Qiu Z, Hou Y, Deng X, Xu W, Zheng T, et al. AXL is a candidate receptor for SARS-CoV-2 that promotes infection of pulmonary and bronchial epithelial cells. Cell Res. 2021;31(2):126-40. Epub 20210108. doi: 10.1038/s41422-020-00460-y. PubMed PMID: 33420426; PubMed Central PMCID: PMCPMC7791157.

49. Gu Y, Cao J, Zhang X, Gao H, Wang Y, Wang J, et al. Receptome profiling identifies KREMEN1 and ASGR1 as alternative functional receptors of SARS-CoV-2. Cell Res. 2022;32(1):24-37. Epub 20211126. doi: 10.1038/s41422-021-00595-6. PubMed PMID: 34837059;

835 PubMed Central PMCID: PMCPMC8617373.

836 50. Cantuti-Castelvetri L, Ojha R, Pedro LD, Djannatian M, Franz J, Kuivanen S, et al.
837 Neuropilin-1 facilitates SARS-CoV-2 cell entry and infectivity. Science. 2020;370(6518):856-60.
838 Epub 20201020. doi: 10.1126/science.abd2985. PubMed PMID: 33082293; PubMed Central
839 PMCID: PMCPMC7857391.

840 51. Khan I, Li S, Tao L, Wang C, Ye B, Li H, et al. Tubeimosides are pan-coronavirus and filovirus
841 inhibitors that can block their fusion protein binding to Niemann-Pick C1. Nat Commun.
842 2024;15(1):162. Epub 20240102. doi: 10.1038/s41467-023-44504-4. PubMed PMID: 38167417;
843 PubMed Central PMCID: PMCPMC10762260.

844 52. Lempp FA, Soriaga LB, Montiel-Ruiz M, Benigni F, Noack J, Park YJ, et al. Lectins enhance
845 SARS-CoV-2 infection and influence neutralizing antibodies. Nature. 2021;598(7880):342-7.
846 Epub 20210831. doi: 10.1038/s41586-021-03925-1. PubMed PMID: 34464958.

847 53. Ou T, Mou H, Zhang L, Ojha A, Choe H, Farzan M. Hydroxychloroquine-mediated inhibition
848 of SARS-CoV-2 entry is attenuated by TMPRSS2. PLoS Pathog. 2021;17(1):e1009212. Epub
849 20210119. doi: 10.1371/journal.ppat.1009212. PubMed PMID: 33465165; PubMed Central
850 PMCID: PMCPMC7845965.

851 54. Essalmani R, Jain J, Susan-Resiga D, Andréo U, Evagelidis A, Derbali RM, et al. Distinctive
852 Roles of Furin and TMPRSS2 in SARS-CoV-2 Infectivity. J Virol. 2022;96(8):e0012822. Epub
853 20220328. doi: 10.1128/jvi.00128-22. PubMed PMID: 35343766; PubMed Central PMCID:
854 PMCPMC9044946.

855 55. Onabajo OO, Banday AR, Stanifer ML, Yan W, Obajemu A, Santer DM, et al. Interferons and
856 viruses induce a novel truncated ACE2 isoform and not the full-length SARS-CoV-2 receptor. Nat
857 Genet. 2020;52(12):1283-93. Epub 20201019. doi: 10.1038/s41588-020-00731-9. PubMed PMID:
858 33077916; PubMed Central PMCID: PMCPMC9377523.

859 56. Ng KW, Attig J, Bolland W, Young GR, Major J, Wrobel AG, et al. Tissue-specific and
860 interferon-inducible expression of nonfunctional ACE2 through endogenous retroelement co-
861 option. Nat Genet. 2020;52(12):1294-302. Epub 20201019. doi: 10.1038/s41588-020-00732-8.
862 PubMed PMID: 33077915; PubMed Central PMCID: PMCPMC7610354.

863 57. Ratnadiwakara M, Änkö ML. mRNA Stability Assay Using transcription inhibition by
864 Actinomycin D in Mouse Pluripotent Stem Cells. Bio Protoc. 2018;8(21):e3072. Epub 20181105.

865 doi: 10.21769/BioProtoc.3072. PubMed PMID: 34532533; PubMed Central PMCID:
866 PMCPMC8342049.

867 58. Huang S, Zhao Y, Phillips S, Warrick Julia E, Kearse Michael G, He C, et al. Single-base
868 m6A epitranscriptomics reveals novel HIV-1 host interaction targets in primary CD4+ T cells.
869 Journal of Virology. 2025;0(0):e01536-25. doi: 10.1128/jvi.01536-25.

870 59. Wang L, Wang S, Wu L, Li W, Bray W, Clark AE, et al. PCIF1-mediated deposition of 5'-cap
871 N(6),2'-O-dimethyladenosine in ACE2 and TMPRSS2 mRNA regulates susceptibility to SARS-
872 CoV-2 infection. Proc Natl Acad Sci U S A. 2023;120(5):e2210361120. Epub 20230123. doi:
873 10.1073/pnas.2210361120. PubMed PMID: 36689652; PubMed Central PMCID:
874 PMCPMC9945940.

875 60. Hopkins TG, Mura M, Al-Ashtal HA, Lahr RM, Abd-Latip N, Sweeney K, et al. The RNA-
876 binding protein LARP1 is a post-transcriptional regulator of survival and tumorigenesis in ovarian
877 cancer. Nucleic Acids Res. 2016;44(3):1227-46. Epub 20151229. doi: 10.1093/nar/gkv1515.
878 PubMed PMID: 26717985; PubMed Central PMCID: PMCPMC4756840.

879 61. Mura M, Hopkins TG, Michael T, Abd-Latip N, Weir J, Aboagye E, et al. LARP1 post-
880 transcriptionally regulates mTOR and contributes to cancer progression. Oncogene.
881 2015;34(39):5025-36. Epub 20141222. doi: 10.1038/onc.2014.428. PubMed PMID: 25531318;
882 PubMed Central PMCID: PMCPMC4430325.

883 62. Wang CW, Chuang HC, Tan TH. ACE2 in chronic disease and COVID-19: gene regulation
884 and post-translational modification. J Biomed Sci. 2023;30(1):71. Epub 20230822. doi:
885 10.1186/s12929-023-00965-9. PubMed PMID: 37608279; PubMed Central PMCID:
886 PMCPMC10464117.

887 63. Liang LJ, Wang D, Yu H, Wang J, Zhang H, Sun BB, et al. Transcriptional regulation and
888 small compound targeting of ACE2 in lung epithelial cells. Acta Pharmacol Sin. 2022;43(11):2895-
889 904. Epub 20220425. doi: 10.1038/s41401-022-00906-6. PubMed PMID: 35468992; PubMed
890 Central PMCID: PMCPMC9035780.

891 64. Senkel S, Lucas B, Klein-Hitpass L, Ryffel GU. Identification of target genes of the
892 transcription factor HNF1beta and HNF1alpha in a human embryonic kidney cell line. Biochim
893 Biophys Acta. 2005;1731(3):179-90. Epub 20051102. doi: 10.1016/j.bbaexp.2005.10.003.
894 PubMed PMID: 16297991.

895 65. Pedersen KB, Chhabra KH, Nguyen VK, Xia H, Lazartigues E. The transcription factor
896 HNF1α induces expression of angiotensin-converting enzyme 2 (ACE2) in pancreatic islets from
897 evolutionarily conserved promoter motifs. Biochim Biophys Acta. 2013;1829(11):1225-35. Epub
898 20131005. doi: 10.1016/j.bbagrm.2013.09.007. PubMed PMID: 24100303; PubMed Central
899 PMCID: PMCPMC3838857.

900 66. Niehof M, Borlak J. HNF4alpha dysfunction as a molecular rational for cyclosporine induced
901 hypertension. PLoS One. 2011;6(1):e16319. Epub 20110127. doi: 10.1371/journal.pone.0016319.
902 PubMed PMID: 21298017; PubMed Central PMCID: PMCPMC3029342.

903 67. Chen L, Marishta A, Ellison CE, Verzi MP. Identification of Transcription Factors Regulating
904 SARS-CoV-2 Entry Genes in the Intestine. Cell Mol Gastroenterol Hepatol. 2021;11(1):181-4.
905 Epub 20200815. doi: 10.1016/j.jcmgh.2020.08.005. PubMed PMID: 32810597; PubMed Central
906 PMCID: PMCPMC7428702.

907 68. Han H, Luo RH, Long XY, Wang LQ, Zhu Q, Tang XY, et al. Transcriptional regulation of
908 SARS-CoV-2 receptor ACE2 by SP1. Elife. 2024;13. Epub 20240220. doi: 10.7554/eLife.85985.
909 PubMed PMID: 38375778; PubMed Central PMCID: PMCPMC10878691.

910 69. Pedersen KB, Chodavarapu H, Lazartigues E. Forkhead Box Transcription Factors of the
911 FOXA Class Are Required for Basal Transcription of Angiotensin-Converting Enzyme 2. J Endocr
912 Soc. 2017;1(4):370-84. Epub 20170306. doi: 10.1210/js.2016-1071. PubMed PMID: 29082356;
913 PubMed Central PMCID: PMCPMC5656262.

914 70. Kuan TC, Yang TH, Wen CH, Chen MY, Lee IL, Lin CS. Identifying the regulatory element
915 for human angiotensin-converting enzyme 2 (ACE2) expression in human cardiofibroblasts.
916 Peptides. 2011;32(9):1832-9. Epub 20110816. doi: 10.1016/j.peptides.2011.08.009. PubMed
917 PMID: 21864606.

918 71. Israeli M, Finkel Y, Yahalom-Ronen Y, Paran N, Chitlaru T, Israeli O, et al. Genome-wide
919 CRISPR screens identify GATA6 as a proviral host factor for SARS-CoV-2 via modulation of ACE2.
920 Nat Commun. 2022;13(1):2237. Epub 20220425. doi: 10.1038/s41467-022-29896-z. PubMed
921 PMID: 35469023; PubMed Central PMCID: PMCPMC9039069.

922 72. Rebendenne A, Roy P, Bonaventure B, Chaves Valadão AL, Desmarets L, Arnaud-Arnould
923 M, et al. Bidirectional genome-wide CRISPR screens reveal host factors regulating SARS-CoV-
924 2, MERS-CoV and seasonal HCoVs. Nat Genet. 2022;54(8):1090-102. Epub 20220725. doi:
925 10.1038/s41588-022-01110-2. PubMed PMID: 35879413; PubMed Central PMCID:

926 PMCPMC11627114.

927 73. Biering SB, Sarnik SA, Wang E, Zengel JR, Leist SR, Schäfer A, et al. Genome-wide
928 bidirectional CRISPR screens identify mucins as host factors modulating SARS-CoV-2 infection.
929 Nat Genet. 2022;54(8):1078-89. Epub 20220725. doi: 10.1038/s41588-022-01131-x. PubMed
930 PMID: 35879412; PubMed Central PMCID: PMCPMC9355872.

931 74. Lau HH, Ng NHJ, Loo LSW, Jasmen JB, Teo AKK. The molecular functions of hepatocyte
932 nuclear factors - In and beyond the liver. J Hepatol. 2018;68(5):1033-48. Epub 20171124. doi:
933 10.1016/j.jhep.2017.11.026. PubMed PMID: 29175243.

934 75. Ng NHJ, Ghosh S, Bok CM, Ching C, Low BSJ, Chen JT, et al. HNF4A and HNF1A exhibit
935 tissue specific target gene regulation in pancreatic beta cells and hepatocytes. Nat Commun.
936 2024;15(1):4288. Epub 20240622. doi: 10.1038/s41467-024-48647-w. PubMed PMID: 38909044;
937 PubMed Central PMCID: PMCPMC11193738.

938 76. Hatzis P, Talianidis I. Regulatory mechanisms controlling human hepatocyte nuclear factor
939 4alpha gene expression. Mol Cell Biol. 2001;21(21):7320-30. doi: 10.1128/mcb.21.21.7320-
940 7330.2001. PubMed PMID: 11585914; PubMed Central PMCID: PMCPMC99906.

941 77. Tian JM, Schibler U. Tissue-specific expression of the gene encoding hepatocyte nuclear
942 factor 1 may involve hepatocyte nuclear factor 4. Genes Dev. 1991;5(12a):2225-34. doi:
943 10.1101/gad.5.12a.2225. PubMed PMID: 1748280.

944 78. Lausen J, Thomas H, Lemm I, Bulman M, Borgschulze M, Lingott A, et al. Naturally occurring
945 mutations in the human HNF4alpha gene impair the function of the transcription factor to a varying
946 degree. Nucleic Acids Res. 2000;28(2):430-7. doi: 10.1093/nar/28.2.430. PubMed PMID:
947 10606640; PubMed Central PMCID: PMCPMC102517.

948 79. Eeckhoute J, Formstecher P, Laine B. Hepatocyte nuclear factor 4alpha enhances the
949 hepatocyte nuclear factor 1alpha-mediated activation of transcription. Nucleic Acids Res.
950 2004;32(8):2586-93. Epub 20040511. doi: 10.1093/nar/gkh581. PubMed PMID: 15141028;
951 PubMed Central PMCID: PMCPMC419469.

952 80. Chu H, Chan JF, Yuen TT, Shuai H, Yuan S, Wang Y, et al. Comparative tropism, replication
953 kinetics, and cell damage profiling of SARS-CoV-2 and SARS-CoV with implications for clinical
954 manifestations, transmissibility, and laboratory studies of COVID-19: an observational study.
955 Lancet Microbe. 2020;1(1):e14-e23. Epub 2020/08/25. doi: 10.1016/s2666-5247(20)30004-5.

956 PubMed PMID: 32835326; PubMed Central PMCID: PMCPMC7173822.

957 81. Yan K, Dumenil T, Tang B, Le TT, Bishop CR, Suhrbier A, et al. Evolution of ACE2-
958 independent SARS-CoV-2 infection and mouse adaption after passage in cells expressing human
959 and mouse ACE2. Virus Evol. 2022;8(2):veac063. Epub 20220727. doi: 10.1093/ve/veac063.
960 PubMed PMID: 35919871; PubMed Central PMCID: PMCPMC9338707.

961 82. Yan K, Dumenil T, Stewart R, Bishop CR, Tang B, Nguyen W, et al. TMEM106B-mediated
962 SARS-CoV-2 infection allows for robust ACE2-independent infection in vitro but not in vivo. Cell
963 Rep. 2024;43(11):114921. Epub 20241031. doi: 10.1016/j.celrep.2024.114921. PubMed PMID:
964 39480813.

965 83. Seamon KJ, Sun Z, Shlyakhtenko LS, Lyubchenko YL, Stivers JT. SAMHD1 is a single-
966 stranded nucleic acid binding protein with no active site-associated nuclease activity. Nucleic
967 Acids Res. 2015;43(13):6486-99. Epub 20150622. doi: 10.1093/nar/gkv633. PubMed PMID:
968 26101257; PubMed Central PMCID: PMCPMC4513882.

969 84. Simermeyer TL, Batalis S, Rogers LC, Zalesak OJ, Hollis T. Protein oxidation increases
970 SAMHD1 binding ssDNA via its regulatory site. Nucleic Acids Res. 2023;51(13):7014-24. doi:
971 10.1093/nar/gkad447. PubMed PMID: 37246644; PubMed Central PMCID: PMCPMC10359594.

972 85. Qian H, Deng X, Huang ZW, Wei J, Ding CH, Feng RX, et al. An HNF1α-regulated feedback
973 circuit modulates hepatic fibrogenesis via the crosstalk between hepatocytes and hepatic stellate
974 cells. Cell Res. 2015;25(8):930-45. Epub 20150714. doi: 10.1038/cr.2015.84. PubMed PMID:
975 26169608; PubMed Central PMCID: PMCPMC4528057.

976 86. Casemayou A, Fournel A, Bagattin A, Schanstra J, Belliere J, Decramer S, et al. Hepatocyte
977 Nuclear Factor-1β Controls Mitochondrial Respiration in Renal Tubular Cells. J Am Soc Nephrol.
978 2017;28(11):3205-17. Epub 20170724. doi: 10.1681/asn.2016050508. PubMed PMID: 28739648;
979 PubMed Central PMCID: PMCPMC5661272.

980 87. Ehle C, Iyer-Bierhoff A, Wu Y, Xing S, Kiehntopf M, Mosig AS, et al. Downregulation of
981 HNF4A enables transcriptomic reprogramming during the hepatic acute-phase response.
982 Commun Biol. 2024;7(1):589. Epub 20240516. doi: 10.1038/s42003-024-06288-1. PubMed PMID:
983 38755249; PubMed Central PMCID: PMCPMC11099168.

984 88. An S, Vo TTL, Son T, Choi H, Kim J, Lee J, et al. SAMHD1-induced endosomal FAK signaling
985 promotes human renal clear cell carcinoma metastasis by activating Rac1-mediated lamellipodia

986 protrusion. Exp Mol Med. 2023;55(4):779-93. Epub 20230403. doi: 10.1038/s12276-023-00961-
987 x. PubMed PMID: 37009792; PubMed Central PMCID: PMCPMC10167369.

988 89. Zhang YY, Liang R, Wang SJ, Ye ZW, Wang TY, Chen M, et al. SARS-CoV-2 hijacks
989 macropinocytosis to facilitate its entry and promote viral spike-mediated cell-to-cell fusion. J Biol
990 Chem. 2022;298(11):102511. Epub 20220919. doi: 10.1016/j.jbc.2022.102511. PubMed PMID:
991 36259516; PubMed Central PMCID: PMCPMC9484108.

992 90. McNab F, Mayer-Barber K, Sher A, Wack A, O'Garra A. Type I interferons in infectious
993 disease. Nat Rev Immunol. 2015;15(2):87-103. doi: 10.1038/nri3787. PubMed PMID: 25614319;
994 PubMed Central PMCID: PMCPMC7162685.

995 91. Yang H, Cheung PH, Wu L. SAMHD1 enhances HIV-1-induced apoptosis in monocytic cells
996 via the mitochondrial pathway. mBio. 2025;16(7):e0042525. Epub 20250528. doi:
997 10.1128/mbio.00425-25. PubMed PMID: 40434097; PubMed Central PMCID:
998 PMCPMC12239581.

999 92. Bonifati S, Daly MB, St Gelais C, Kim SH, Hollenbaugh JA, Shepard C, et al. SAMHD1
1000 controls cell cycle status, apoptosis and HIV-1 infection in monocytic THP-1 cells. Virology.
1001 2016;495:92-100. Epub 20160514. doi: 10.1016/j.virol.2016.05.002. PubMed PMID: 27183329;
1002 PubMed Central PMCID: PMCPMC4912869.

1003 93. Odle A, Kar M, Verma AK, Sariol A, Meyerholz DK, Suthar MS, et al. Tissue-resident memory
1004 T cells contribute to protection against heterologous SARS-CoV-2 challenge. JCI Insight.
1005 2024;9(23). Epub 20241206. doi: 10.1172/jci.insight.184074. PubMed PMID: 39405115; PubMed
1006 Central PMCID: PMCPMC11623939.

1007 94. Owczarzy R, Tataurov AV, Wu Y, Manthey JA, McQuisten KA, Almabrazi HG, et al. IDT
1008 SciTools: a suite for analysis and design of nucleic acid oligomers. Nucleic Acids Res.
1009 2008;36(Web Server issue):W163-9. Epub 20080425. doi: 10.1093/nar/gkn198. PubMed PMID:
1010 18440976; PubMed Central PMCID: PMCPMC2447751.

1011 95. Wong LR, Zheng J, Wilhelmsen K, Li K, Ortiz ME, Schnicker NJ, et al. Eicosanoid signalling
1012 blockade protects middle-aged mice from severe COVID-19. Nature. 2022;605(7908):146-51.
1013 Epub 20220321. doi: 10.1038/s41586-022-04630-3. PubMed PMID: 35314834; PubMed Central
1014 PMCID: PMCPMC9783543.

1015 96. Phillips S, Mishra T, Khadka S, Bohan D, Espada CE, Maury W, et al. Epitranscriptomic N(6)-

1016 Methyladenosine Profile of SARS-CoV-2-Infected Human Lung Epithelial Cells. Microbiol Spectr.
1017 2023;11(1):e0394322. Epub 20230110. doi: 10.1128/spectrum.03943-22. PubMed PMID:
1018 36625663; PubMed Central PMCID: PMCPMC9927293.

1019 97. Cheung PH, Ye ZW, Lui WY, Ong CP, Chan P, Lee TT, et al. Production of single-cycle
1020 infectious SARS-CoV-2 through a trans-complemented replicon. J Med Virol. 2022;94(12):6078-
1021 90. Epub 20220817. doi: 10.1002/jmv.28057. PubMed PMID: 35941087; PubMed Central PMCID:
1022 PMCPMC9539037.

1023 98. Mehyar N, Samman N, Al Gheribi S, Mashhour A, Chan P, Al-Kaysi RO, et al. First-in-class
1024 inhibitors of Nsp15 endoribonuclease of SARS-CoV-2: Modeling, synthesis, and enzymatic assay
1025 of thiazolidinedione and rhodanine analogs. J Biol Chem. 2025;301(8):110409. Epub 20250623.
1026 doi: 10.1016/j.jbc.2025.110409. PubMed PMID: 40562099; PubMed Central PMCID:
1027 PMCPMC12303054.

1028 99. Corman VM, Landt O, Kaiser M, Molenkamp R, Meijer A, Chu DK, et al. Detection of 2019
1029 novel coronavirus (2019-nCoV) by real-time RT-PCR. Euro Surveill. 2020;25(3). doi:
1030 10.2807/1560-7917.Es.2020.25.3.2000045. PubMed PMID: 31992387; PubMed Central PMCID:
1031 PMCPMC6988269.

1032 100. Zhao LM, Zheng ZX, Zhao X, Shi J, Bi JJ, Pei W, et al. Optimization of reference genes for
1033 normalization of the quantitative polymerase chain reaction in tissue samples of gastric cancer.
1034 Asian Pac J Cancer Prev. 2014;15(14):5815-8. doi: 10.7314/apjcp.2014.15.14.5815. PubMed
1035 PMID: 25081706.

1036 101. Chan P, Ye ZW, Zhao W, Ong CP, Sun XY, Cheung PH, et al. Mpox virus poxin-schlafen
1037 fusion protein suppresses innate antiviral response by sequestering STAT2. Emerg Microbes
1038 Infect. 2025;14(1):2477639. Epub 20250318. doi: 10.1080/22221751.2025.2477639. PubMed
1039 PMID: 40066622; PubMed Central PMCID: PMCPMC11921170.

1040 102. Spandidos A, Wang X, Wang H, Seed B. PrimerBank: a resource of human and mouse PCR
1041 primer pairs for gene expression detection and quantification. Nucleic Acids Res.
1042 2010;38(Database issue):D792-9. Epub 20091111. doi: 10.1093/nar/gkp1005. PubMed PMID:
1043 19906719; PubMed Central PMCID: PMCPMC2808898.

1044

1045 **Figure legends of 9 main figures**

1046 **Figure 1. Generation and characterization of SAMHD1 KO Calu-3 cell lines.** (A) Schematic
1047 diagram of human SAMHD1 protein domains showing the target sites of sgRNA1 or sgRNA2. (B)
1048 SAMHD1 expression of Calu-3 cells transduced to express SpCas9 without the expression of any
1049 sgRNA (Ctrl, two single clones) or with the expression of sgRNA1 (five single clones) or sgRNA2
1050 (three single clones). GAPDH detection was used as normalization control. The relative band
1051 intensities of SAMHD1 were calculated by dividing them with GAPDH bands and were normalized
1052 to Ctrl clone 1. Clone 1 of Ctrl, clone 4 of sgRNA1- and clone 3 of sgRNA 2- treated groups were
1053 chosen for all subsequent experiments and respectively named Ctrl, KO1 and KO2. (C) Levels of
1054 IL-6, IFNβ, OAS1 and ISG15 mRNA were measured with RT-qPCR. 18S RNA was used as
1055 internal control. Biological sextuplicate experiments were performed. One-way ANOVA multiple
1056 comparisons test was used to evaluate the statistical significance of the difference between Ctrl
1057 and KO1 or KO2. * $P<0.05$, *** $P<0.001$, **** $P<0.0001$. ns, not significant.

1058

1059 **Figure 2. Suppression of SARS-CoV-2 infection by SAMHD1 depletion independent to IFN**
1060 **antiviral response.** (A, B) Calu-3 Ctrl, KO1 or KO2 cells were infected with authentic SARS-CoV-
1061 2 at MOI=0.05. Culture supernatant was collected at 0, 24, 48 or 72 hpi. (A) Infectious titer or (B)
1062 viral copy number of the conditioned media were respectively measured by plaque assay or RT-

1063 qPCR. Statistical comparison was performed at each time point between Ctrl and KO1 or KO2.
1064 (C) Viral N and S proteins of infected Ctrl, KO1 or KO2 cells (SARS-CoV-2, MOI=1) were detected
1065 at 24 hpi. GAPDH was detected as an input control. The relative band intensities of viral N and
1066 viral S were calculated by dividing them with GAPDH bands and were normalized to Ctrl cells. (D)
1067 The levels of viral RNA (N), IFNβ mRNA, IFNλ mRNA and OAS1 mRNA of infected Ctrl, KO1 or
1068 KO2 cells (SARS-CoV-2, MOI=1, 0 or 24 hpi) were quantified with RT-qPCR. 18S RNA was used
1069 as internal control. (E, F and G) Calu-3 Ctrl, KO1 or KO2 cells treated with 10 μM baricitinib or
1070 DMSO (added 4 hrs before infection) were infected with authentic SARS-CoV-2 at MOI=1. At 24
1071 hpi, culture supernatant, cellular protein and cellular RNA were harvested and respectively tested
1072 with (E) plaque assay, (F) Western blot or (G) RT-qPCR. For (F), viral N protein, total STAT1 or
1073 S727-phosphorylated STAT1 (p-STAT1) were detected and GAPDH was used as input control.
1074 The relative band intensities of viral N, STAT1, or p-STAT1 were calculated by dividing them with
1075 GAPDH bands and were normalized to Ctrl cells treated with DMSO. For (G), viral N RNA and
1076 OAS1 mRNA were detected. 18S RNA was used as normalization control. For (A), (B), (D) and
1077 (G), biological triplicate experiment was performed. For (E), biological quadruplicate experiment
1078 was performed. For (A), (B), (D), (E) and (G), two-way ANOVA multiple comparisons test was
1079 performed. * $P<0.05$, ** $P<0.01$, *** $P<0.001$, **** $P<0.0001$. ns, not significant.
1080

1081 **Figure 3. SAMHD1 depletion suppresses spike protein-mediated viral entry.** (A) Viral RNA
1082 levels (N and E genes) of Calu-3 Ctrl cells infected with ΔS-VRP(G) at 1.2 x 10^5 copy number per
1083 cell and treated with 5 μM remdesivir (RDV) or DMSO were quantified with RT-qPCR at 24 hpi.
1084 18S RNA was used as normalization control. Biological triplicate experiments were performed. (B,
1085 C and D) Calu-3 Ctrl, KO1 or KO2 cells were infected with ΔS-VRP(G) at 1.2 x 10^5 copy number
1086 per cell. (B) Viral RNA levels (N and E genes) were quantified with RT-qPCR at indicated time
1087 points. 18S RNA was used as normalization control. Biological triplicate experiments were
1088 performed. (C) Viral N protein was detected with Western blot at indicated time points. GAPDH
1089 was used as input control. The relative band intensities of viral N were calculated by dividing them
1090 with GAPDH bands and were normalized to Ctrl cells at 24 hpi. (D) The activities of secreted
1091 *Guassia* luciferase at indicated time points were assayed through Pierce™ *Gaussia* Luciferase
1092 Flash Assay Kit. Biological quadruplicate experiments were performed. (E) Cellular luciferase
1093 activities of HIV-1-spike-Luc/ZsGreen infected Calu-3 Ctrl, KO1 or KO2 cells (12.5 $TCID_{50}$ per cell)
1094 were measured at 48 hpi. Biological sextuplicate experiments were performed. For (A), (B) and
1095 (D), two-way ANOVA multiple comparisons test was performed. For (E), one-way ANOVA multiple
1096 comparisons test was used. * $P<0.05$, ** $P<0.01$, *** $P<0.001$. ns, not significant.
1097
1098 **Figure 4. SAMHD1 depletion downregulates the expression of SARS-CoV-2 receptor ACE2.**

1099 (A) Calu-3 Ctrl, KO1 and KO2 cells were subjected to mRNA-Seq using Element Aviti24.
1100 Biological triplicate was performed. DEGs were identified and selected based on the following
1101 criteria: FDR-adjusted P <0.01 and $\log_2$ fold change >1. The number of DEGs in the three different
1102 comparison groups were plotted on a Venn diagram (i.e. Ctrl vs KO1, Ctrl vs KO2 and KO1 vs
1103 KO2). 681 common DEGs of Ctrl vs KO1 and Ctrl vs KO2 were found to have consistent direction
1104 of change. (B) The 681 DEGs described in (A) were plotted on two volcano plots with FDR-
1105 adjusted P values against $\log_2$ fold change according to the values of KO1 vs Ctrl (left) or KO2 vs
1106 Ctrl (right). Three known viral entry factors ACE2, TMPRSS2 and Furin were identified. The values
1107 of $\log_2$ fold change were labelled adjacent to the corresponding data points. (C) mRNA levels of
1108 ACE2 (primer pair 1, Table S5) and TMPRSS2 of Ctrl, KO1 or KO2 cells were quantified with RT-
1109 qPCR. 18S RNA was used as normalization control. Biological sextuplicate experiments were
1110 performed. (D) Protein levels of ACE2 and TMPRSS2 were measured with Western blot. GAPDH
1111 was used as the input control. Triangle (◁) and asterisk (*) symbols respectively represented the
1112 zymogen (~55 kDa) and active form (~31 kDa) of TMPRSS2. The relative band intensities of
1113 ACE2, TMPRSS2 zymogen and TMPRSS2 active form were calculated by dividing them with
1114 GAPDH bands and were normalized to Ctrl. For (C), one-way ANOVA multiple comparisons test
1115 was used to evaluate the statistical significance of the difference between Ctrl and KO1 or KO2.
1116 **** P<0.0001, ns, not significant.

1117

1118 **Figure 5. SAMHD1 KO does not affect ACE2 mRNA stability.** (A-C) The levels of ACE2 mRNA

1119 of actinomycin D (10 μg/mL) treated Calu-3 Ctrl, KO1 or KO2 cells were quantified with RT-qPCR

1120 using (A) primer pair 1, (B) primer pair 2 or (C) primer pair 3 (Table S5) at indicated time points.

1121 (D) BIK mRNA and (E) 18S RNA were detected with RT-qPCR as controls to the experiment. Total

1122 RNA (1 μg) was used for reverse transcription. mRNA levels were normalized to 0 hr. The one

1123 phase decay curves for KO1 (blue), KO2 (red) and Ctrl cells (black) were plotted.

1124

1125 **Figure 6. SAMHD1 KO decreases the expression HNF1α, HNF1β and HNF4α.** mRNA levels

1126 of (A) HNF1α, (B) HNF1β, (C) HNF4α and (D) GATA6 were measured with RT-qPCR. 18S RNA

1127 was used as normalization control. (E) Protein levels of HNF1α, HNF1β and HNF4α were

1128 detected with Western blot. GAPDH was detected for input control. The relative band intensities

1129 of HNF1α, HNF1β and HNF4α were calculated by dividing them with GAPDH bands and were

1130 normalized to Ctrl cells. For (A)-(D), one-way ANOVA multiple comparisons test was used to

1131 evaluate the statistical significance of the difference between Ctrl and KO1 or KO2. ** $P<0.01$, ***

1132 $P<0.001$, **** $P<0.0001$. ns, not significant.

1133

1134 **Figure 7. Knocking down HNF1α and HNF1β downregulates ACE2 expression and**

1135 **suppresses SARS-CoV-2 infection.** (A) ACE2, HNF1α, HNF1β or HNF4α proteins of Calu-3

1136 cells (4 x 10^5) treated with DsiRNA (24 pmol, 72 hpt) targeting HNF1α, HNF1β, HNF4α or NC

1137 were detected with Western blot. GAPDH was detected for input control. A representative blot

1138 was shown. (B) ACE2, HNF1α, HNF1β or HNF4α protein band intensities of three independent

1139 experiments (i.e. (A) and Supplementary S4A) were quantified by densitometry analysis and

1140 divided by GAPDH and normalized to NC control. (C) Cells were treated similarly as in (A). The

1141 mRNA levels of ACE2 (primer pair 1, Table S5), HNF1α, HNF1β or HNF4α were quantified with

1142 RT-qPCR. 18S RNA was used as normalization control. (D) Calu-3 cells (3.2 x 10^6) transfected

1143 DsiRNA (192 pmol, 72 hpt) targeting HNF1α, HNF1β or NC were infected with authentic SARS-

1144 CoV-2 at MOI=0.05. Released viral progenies in culture supernatants were quantified with plaque

1145 assay. Biological triplicate experiments were performed. For (B-C), unpaired T-test was used to

1146 evaluate the statistical significance of the difference between sample groups and NC. For (D),

1147 two-way ANOVA multiple comparisons test was performed comparing Ctrl and KO1 or KO2 at

1148 various time points. * $P<0.05$, ** $P<0.01$, *** $P<0.001$, **** $P<0.0001$. ns, not significant.

1149

1150 **Figure 8. SAMHD1 deficiency mitigates the effect of HNF1α and HNF1β knockdown in**

1151 **further suppressing ACE2 expression.** (A) ACE2, HNF1α and HNF1β proteins of Ctrl, KO1 or

1152 KO2 cells (2 x 10^5) treated with DsiRNA (12 pmol, 72 hpt) targeting HNF1α, HNF1β or NC were

1153 detected with Western blot. GAPDH was detected for input control. A representative blot was
1154 shown. (B) HNF1α, (C) HNF1β and (D) ACE2 protein band intensities of three independent
1155 experiments (i.e. (A) and Supplementary S4B) were quantified by densitometry analysis, divided
1156 by GAPDH bands and normalized to Ctrl NC. (E) Cells were treated similarly as in (A). The mRNA
1157 levels of ACE2 (primer pair 1, Table S5) were quantified with RT-qPCR. 18S RNA was used as
1158 normalization control. One-way ANOVA multiple comparisons test was used to evaluate the
1159 statistical significance of the difference between sample groups. * P<0.05, ** P<0.01, *** P<0.001,
1160 **** P<0.0001. ns, not significant.
1161
1162 **Figure 9. SAMHD1 promotes SARS-CoV-2 infection via HNF1-mediated ACE2 expression.**
1163 SAMHD1 supports the expression of HNF1α and HNF1β which respectively promote mRNA and
1164 protein expression of ACE2 in human lung epithelial cells (Calu-3). Upon infection, SARS-CoV-2
1165 binds to ACE2 receptor via its surface spike protein to initiate viral entry. In the absence of
1166 SAMHD1 expression (i.e. SAMHD1 KO), cellular stresses are induced such as proinflammatory
1167 cytokine expression (thunder symbols). The expression levels of HNF1α and HNF1β are reduced.
1168 In turn, ACE2 expression is reduced which blocks SARS-CoV-2 infection via spike protein-
1169 mediated viral entry. Whether and how proinflammatory cytokines produced by SAMHD1 KO
1170 Calu-3 cells (e.g. IL-6, IL-1, CSF2, or IL-11) suppress HNF-1-mediated ACE2 expression remains

1171 unclear and requires further studies.

1172

1173 **Figure legends of 5 supplementary figures**

1174

1175 **Supplementary Fig. S1. Validation of SAMHD1 deficiency in SAMHD1 KO Calu-3 cells.** (A
1176 and B) The sanger sequencing results to the regions of SpCas9 cleavage sites directed by
1177 respectively sgRNA1 or sgRNA2 of (A) KO1 and (B) KO2 cells were shown and compared with
1178 that of the Ctrl cells. Red arrows indicated one base pair insertion near the SpCas9 cleavage site.
1179 (C) dATP levels of Calu-3 Ctrl, KO1 or KO2 cells were measured with HIV-1 RT based single
1180 nucleotide incorporation assay. For (C), one-way ANOVA multiple comparisons test was used to
1181 evaluate the statistical significance of the difference between Ctrl and KO1 or KO2. ** $P<0.01$. ns,
1182 not significant.

1183

1184 **Supplementary Fig. S2. PCA clustering of Calu-3 Ctrl, KO1 and KO2 cells based on the**
1185 **mRNA-seq profiles.** Nine samples of the mRNA-seq analysis gave nine PCs (i.e. Ctrl, KO1 and
1186 KO2 cells, biological triplicate). The influence of each PC was plotted based on their contributing
1187 variance (%). The cumulative variances from 1 to 9 were plotted above and joined by a curve.
1188 PC1 and PC2 gave 98% coverage of all PCs. (B) Individual samples from Ctrl, KO1 and KO2

1189 cells were plotted along the PC1 and PC2 based on the net scores of loading genes obtained

1190 from PCA. (C) A PCA biplot was generated by top ten loading genes influencing PC1 and PC2.

1191

1192 **Supplementary Fig. S3. Confirming ACE2 and dACE2 mRNA expressions in SAMHD1 KO**

1193 **Calu-3 cells.** The mRNA levels of (A) ACE2 and (B) dACE2 of Ctrl, KO1 and KO2 cells were

1194 measured by RT-qPCR with qPCR primer pairs previously described [55]. For ACE2, primer pair

1195 4 listed in Table S5 was used. Biological triplicate experiment was performed. One-way ANOVA

1196 multiple comparisons test was used to evaluate the statistical significance of the difference

1197 between Ctrl and KO1 or KO2. ** $P<0.01$, *** $P<0.001$. ns, not significant.

1198

1199 **Supplementary Fig. S4. Independent experiments performed for protein band calculation**

1200 **of Fig. 7B and Fig. 8B-8D.** The Western blot results to two more independent experiment

1201 replicates for the same experiment conducted in Fig. 7A and Fig. 8A were respectively shown in

1202 (A) and (B).

1203

1204 **Supplementary Fig. S5. Gene ontology enrichment analysis to cellular components to the**

1205 **common DEGs of SAMHD1 KO Calu-3 cells.** 681 consistent DEGs obtained from SAMHD1 KO

1206 Calu-3 cells as shown in Fig. 4A were used for gene ontology enrichment analysis to the category

1207 of “Cellular component”. Top ten GO terms with the best FDR-adjusted P values were plotted on

1208 a bubble plot against the rich ratio (i.e. number of DEGs per all annotated genes of the GO term).

1209 The number of counts of DEGs was shown in terms of the size of the bubble. The bubble plot was

1210 generated with the online resources SR plot (https://www.bioinformatics.com.cn/srplot).

1211

1212 **Information of supplementary Table S1-S5**

1213 **Supplementary Table S1.** DEGs observed in the mRNA-seq data sets on the three comparison

1214 pairs (Ctrl vs KO1, Ctrl vs KO2 and KO1 vs KO2 cells).

1215

1216 **Supplementary Table S2.** The 681 common DEGs observed in both Calu-3 KO1 and KO2 cells

1217 as shown in Fig. 4A.

1218

1219 **Supplementary Table S3.** All GO terms in the category of “Cellular component” enriched based

1220 on the 681 common DEGs shown in Fig. 4A.

1221

1222 **Supplementary Table S4.** Enriched DEGs of the top ten GO terms as shown in Fig. S5.

1223

1224 **Supplementary Table S5.** DsiRNA and RT-qPCR primer sequences and related information.

Fig. 1

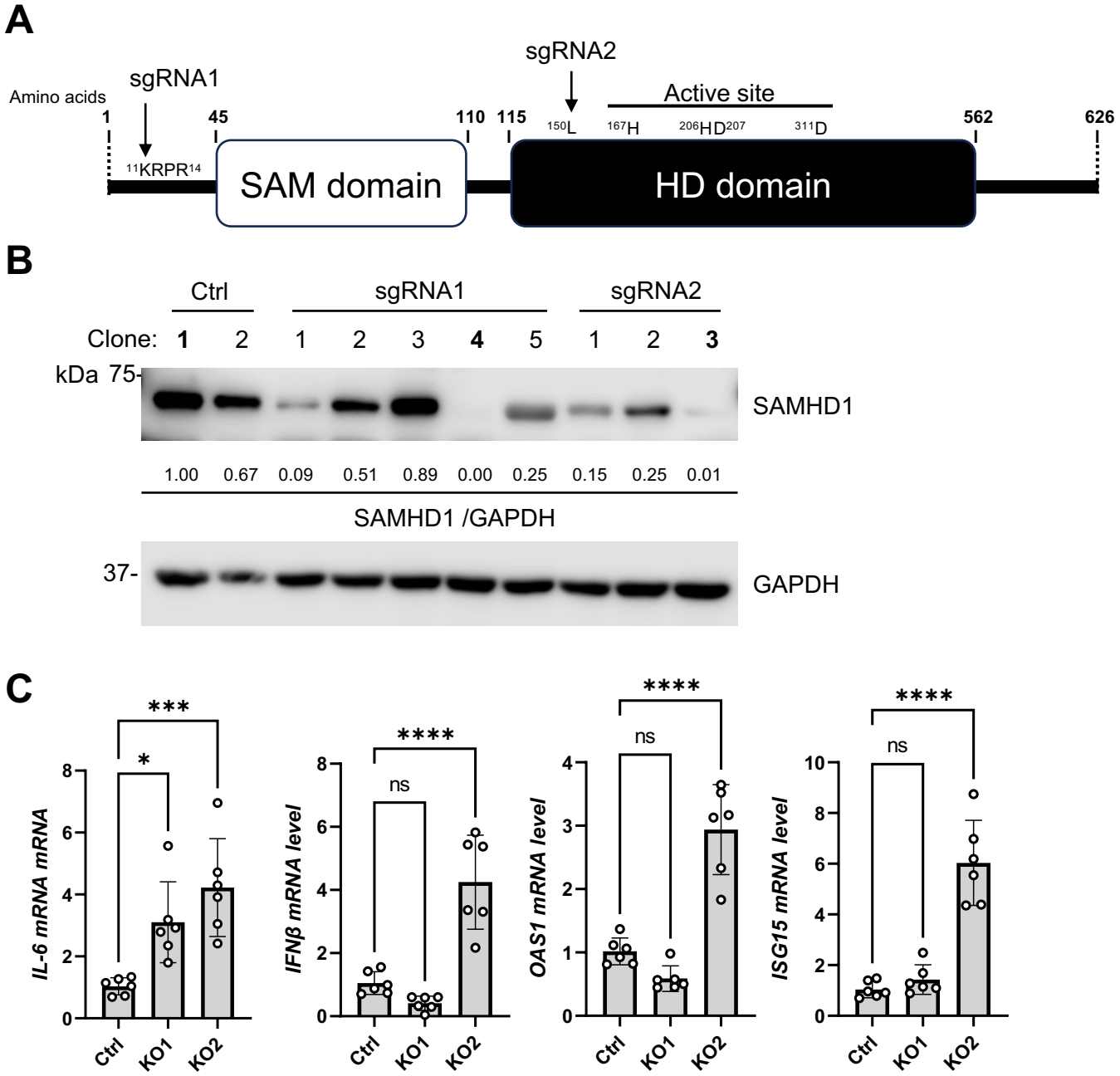
A
sgRNA1
sgRNA2
Amino acids
1
45
110
115
150L
167H
206HD207
311D
562
626
11KRPR14
Active site
SAM domain
HD domain
B
Ctrl
sgRNA1
sgRNA2
Clone: 1 2 1 2 3 4 5 1 2 3
kDa 75-
SAMHD1
1.00 0.67 0.09 0.51 0.89 0.00 0.25 0.15 0.25 0.01
SAMHD1 /GAPDH
37-
GAPDH
C
IL-6 mRNA mRNA
IFNβ mRNA level
OAS1 mRNA level
ISG15 mRNA level
***
*
****
ns
Ctrl
KO1
KO2

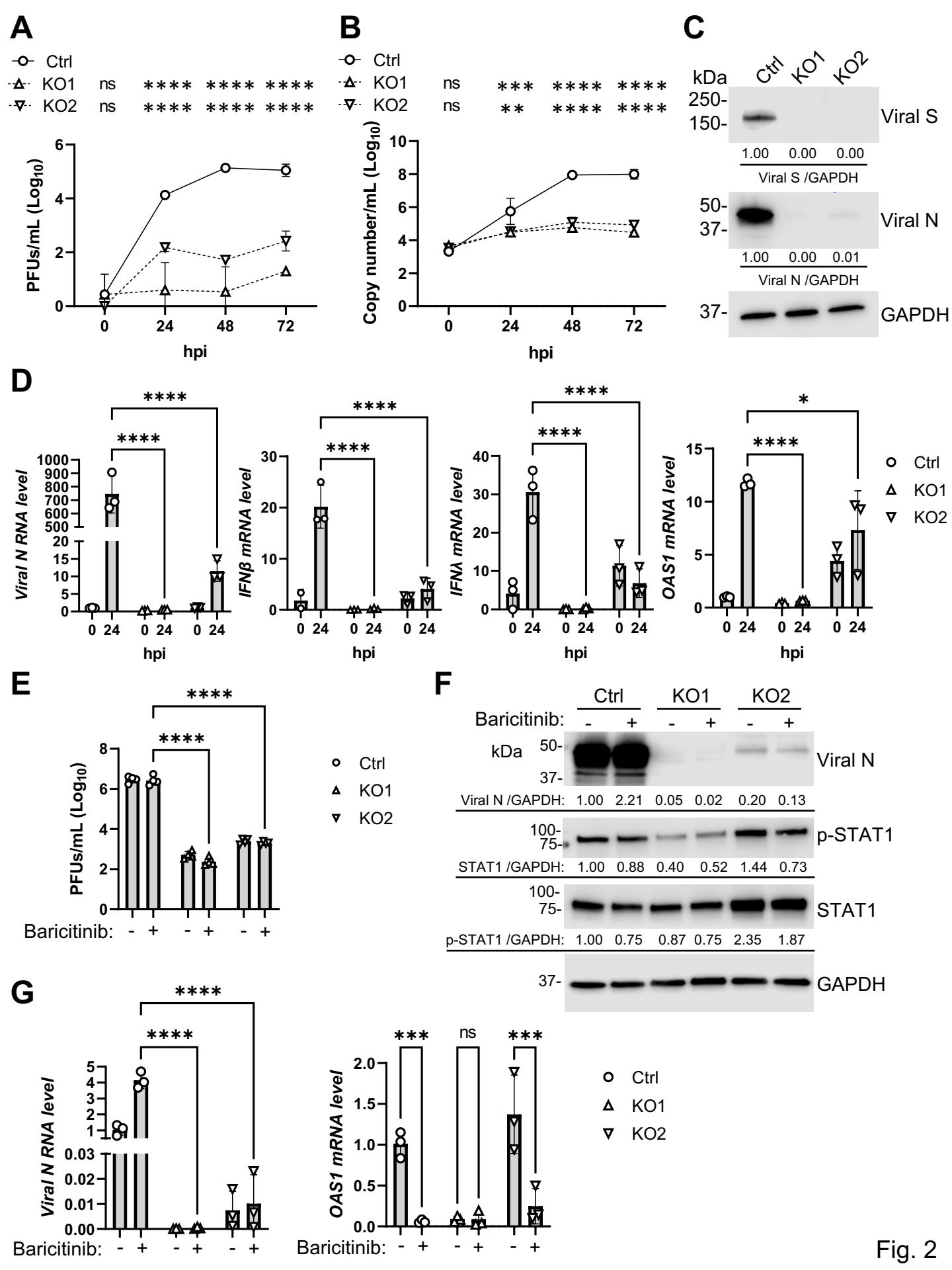
A
Ctrl
KO1 ns **** **** ****
KO2 ns **** **** ****
PFUs/mL (Log10)
hpi
B
Ctrl
KO1 ns *** **** ****
KO2 ns ** **** ****
Copy number/mL (Log10)
hpi
C
kDa
Ctrl KO1 KO2
250-
150-
Viral S
1.00 0.00 0.00
Viral S /GAPDH
50-
37-
Viral N
1.00 0.00 0.01
Viral N /GAPDH
37-
GAPDH
D
Viral N RNA level
IFNβ mRNA level
IFNA mRNA level
OAS1 mRNA level
hpi
Ctrl
KO1
KO2
E
PFUs/mL (Log10)
Baricitinib: - + - + - +
Ctrl
KO1
KO2
F
Ctrl KO1 KO2
Baricitinib: - + - + - +
kDa
50-
37-
Viral N
Viral N /GAPDH: 1.00 2.21 0.05 0.02 0.20 0.13
100-
75-
p-STAT1
STAT1 /GAPDH: 1.00 0.88 0.40 0.52 1.44 0.73
100-
75-
STAT1
p-STAT1 /GAPDH: 1.00 0.75 0.87 0.75 2.35 1.87
37-
GAPDH
G
Viral N RNA level
OAS1 mRNA level
Baricitinib: - + - + - +
Ctrl
KO1
KO2

Fig. 2

Fig. 3

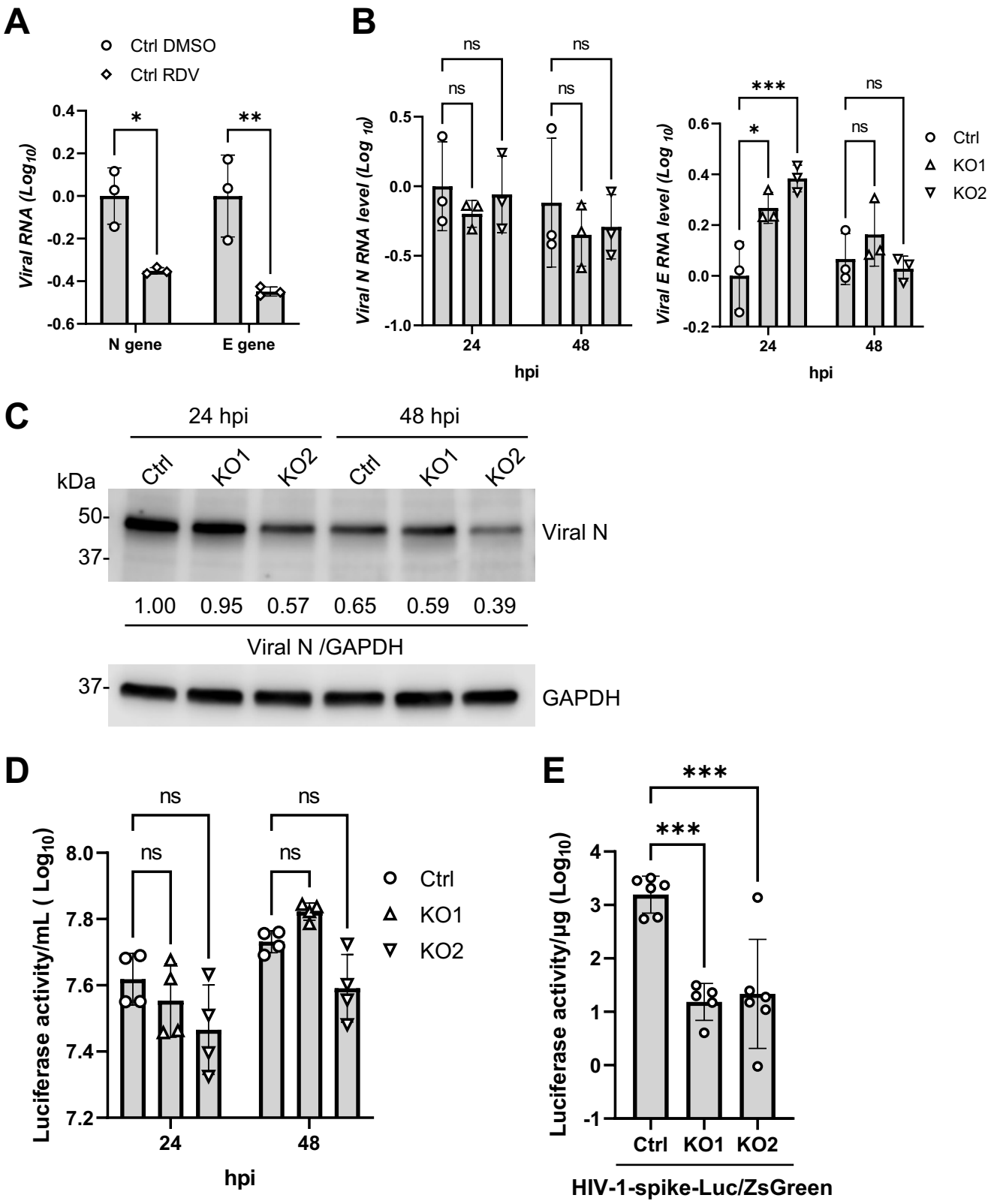
A
Ctrl DMSO
Ctrl RDV
Viral RNA (Log10)
N gene
E gene
B
Viral N RNA level (Log 10)
Viral E RNA level (Log 10)
ns
***
*
**
24
48
hpi
Ctrl
KO1
KO2
C
24 hpi
48 hpi
kDa
50-
37-
Viral N
1.00 0.95 0.57 0.65 0.59 0.39
Viral N /GAPDH
GAPDH
D
Luciferase activity/mL (Log10)
E
Luciferase activity/µg (Log10)
HIV-1-spike-Luc/ZsGreen

Fig. 4

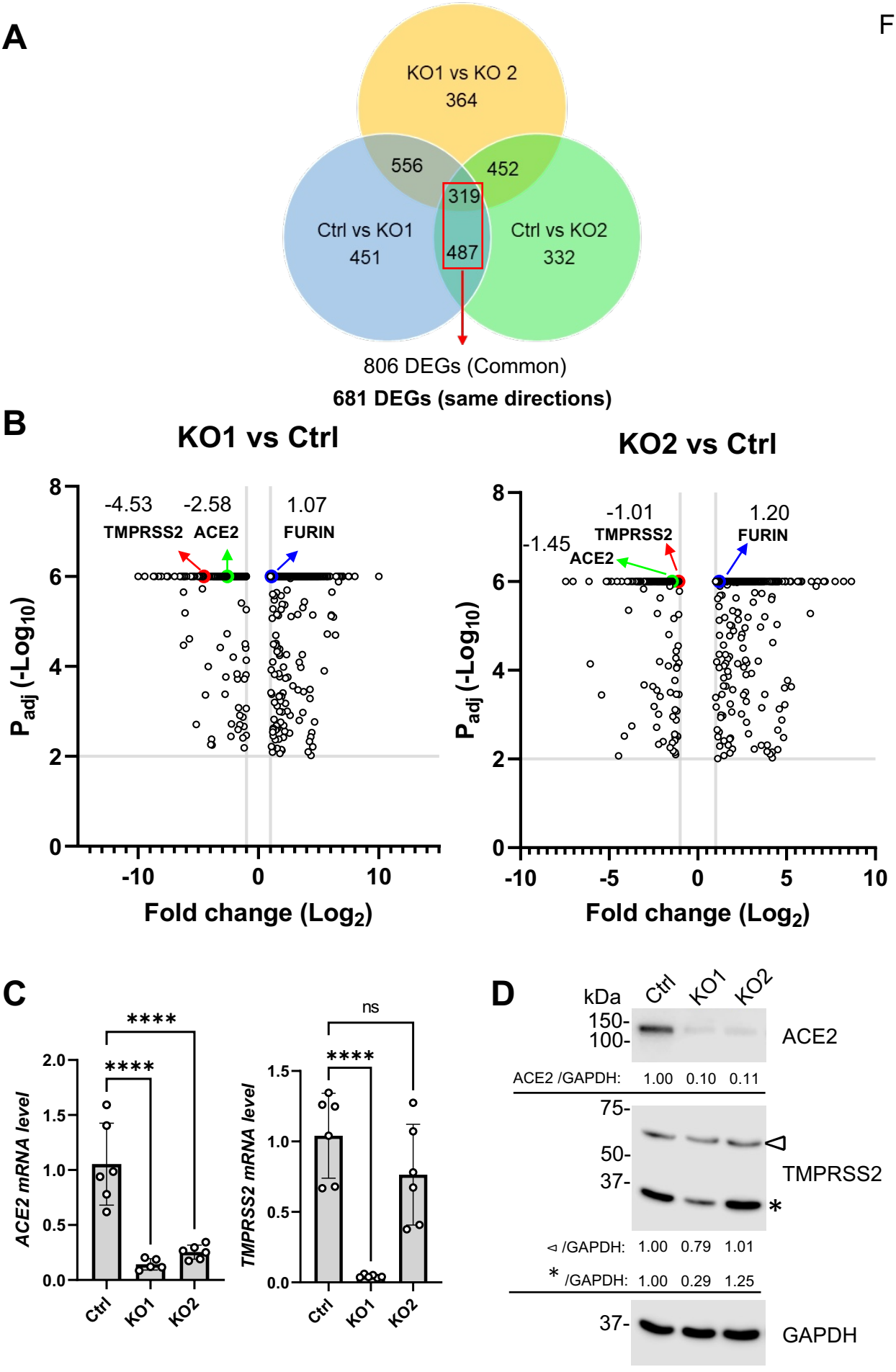
A
KO1 vs KO 2
364
556
452
319
Ctrl vs KO1
451
487
Ctrl vs KO2
332
806 DEGs (Common)
681 DEGs (same directions)
B
KO1 vs Ctrl
-4.53
-2.58
1.07
TMPRSS2
ACE2
FURIN
Padj (-Log10)
Fold change (Log2)
KO2 vs Ctrl
-1.01
1.20
-1.45
TMPRSS2
ACE2
FURIN
Padj (-Log10)
Fold change (Log2)
C
****
****
ACE2 mRNA level
Ctrl
KO1
KO2
ns
****
TMPRSS2 mRNA level
Ctrl
KO1
KO2
D
kDa
Ctrl
KO1
KO2
150-
100-
ACE2
ACE2 /GAPDH: 1.00 0.10 0.11
75-
50-
37-
TMPRSS2
◁ /GAPDH: 1.00 0.79 1.01
* /GAPDH: 1.00 0.29 1.25
37-
GAPDH

Fig. 5

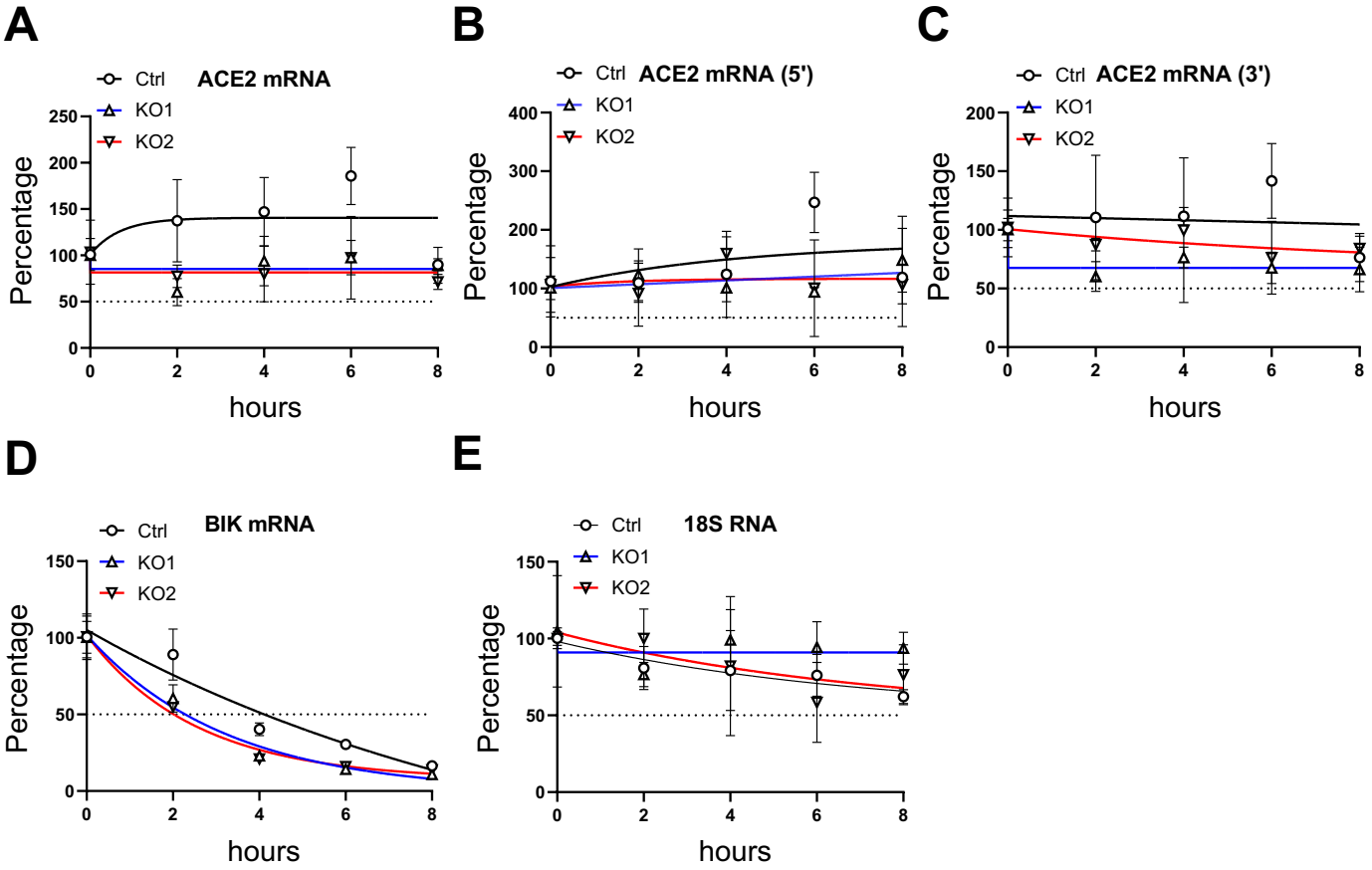
A
ACE2 mRNA
Ctrl
KO1
KO2
Percentage
hours
B
ACE2 mRNA (5')
Ctrl
KO1
KO2
Percentage
hours
C
ACE2 mRNA (3')
Ctrl
KO1
KO2
Percentage
hours
D
BIK mRNA
Ctrl
KO1
KO2
Percentage
hours
E
18S RNA
Ctrl
KO1
KO2
Percentage
hours

Fig. 6

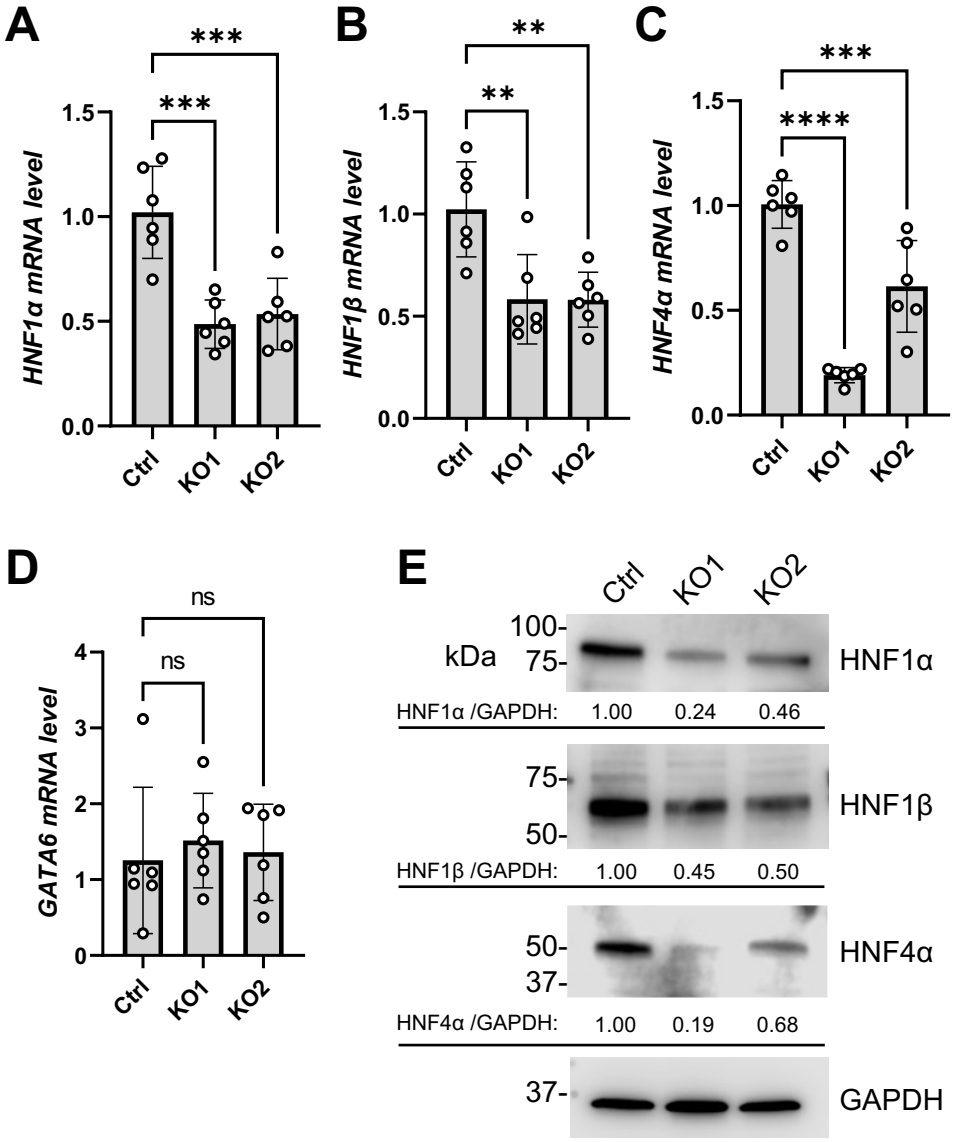
A
B
C
D
E
HNF1α mRNA level
HNF1β mRNA level
HNF4α mRNA level
GATA6 mRNA level
Ctrl
KO1
KO2
***
**
****
ns
kDa
100-
75-
50-
37-
HNF1α
HNF1β
HNF4α
GAPDH
HNF1α /GAPDH: 1.00 0.24 0.46
HNF1β /GAPDH: 1.00 0.45 0.50
HNF4α /GAPDH: 1.00 0.19 0.68

Fig. 7

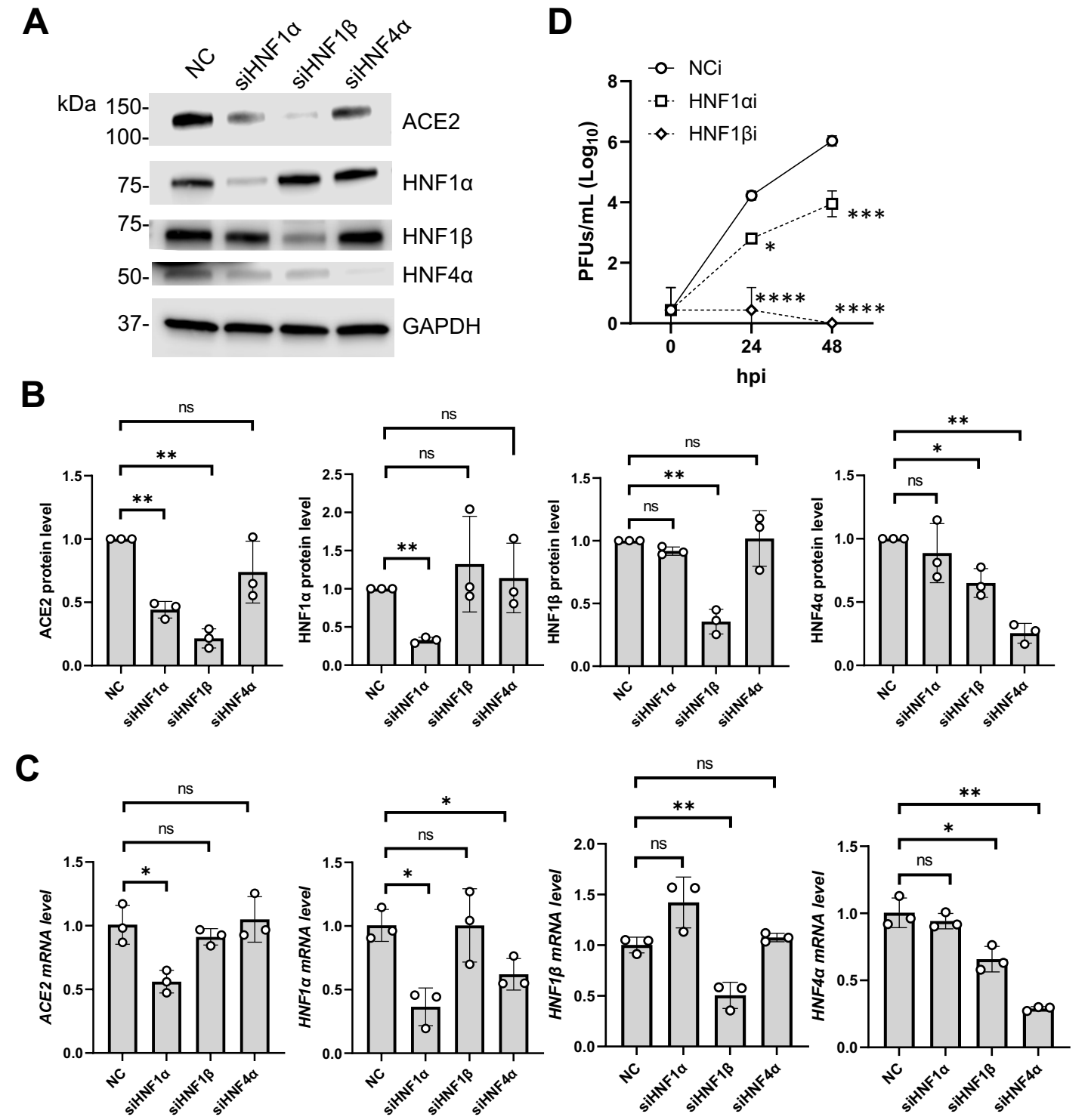
A
NC
siHNF1α
siHNF1β
siHNF4α
kDa
150-
100-
75-
75-
50-
37-
ACE2
HNF1α
HNF1β
HNF4α
GAPDH
D
NCi
HNF1αi
HNF1βi
PFUs/mL (Log10)
hpi
B
ACE2 protein level
HNF1α protein level
HNF1β protein level
HNF4α protein level
C
ACE2 mRNA level
HNF1α mRNA level
HNF1β mRNA level
HNF4α mRNA level
ns
NC
siHNF1α
siHNF1β
siHNF4α

Fig. 8

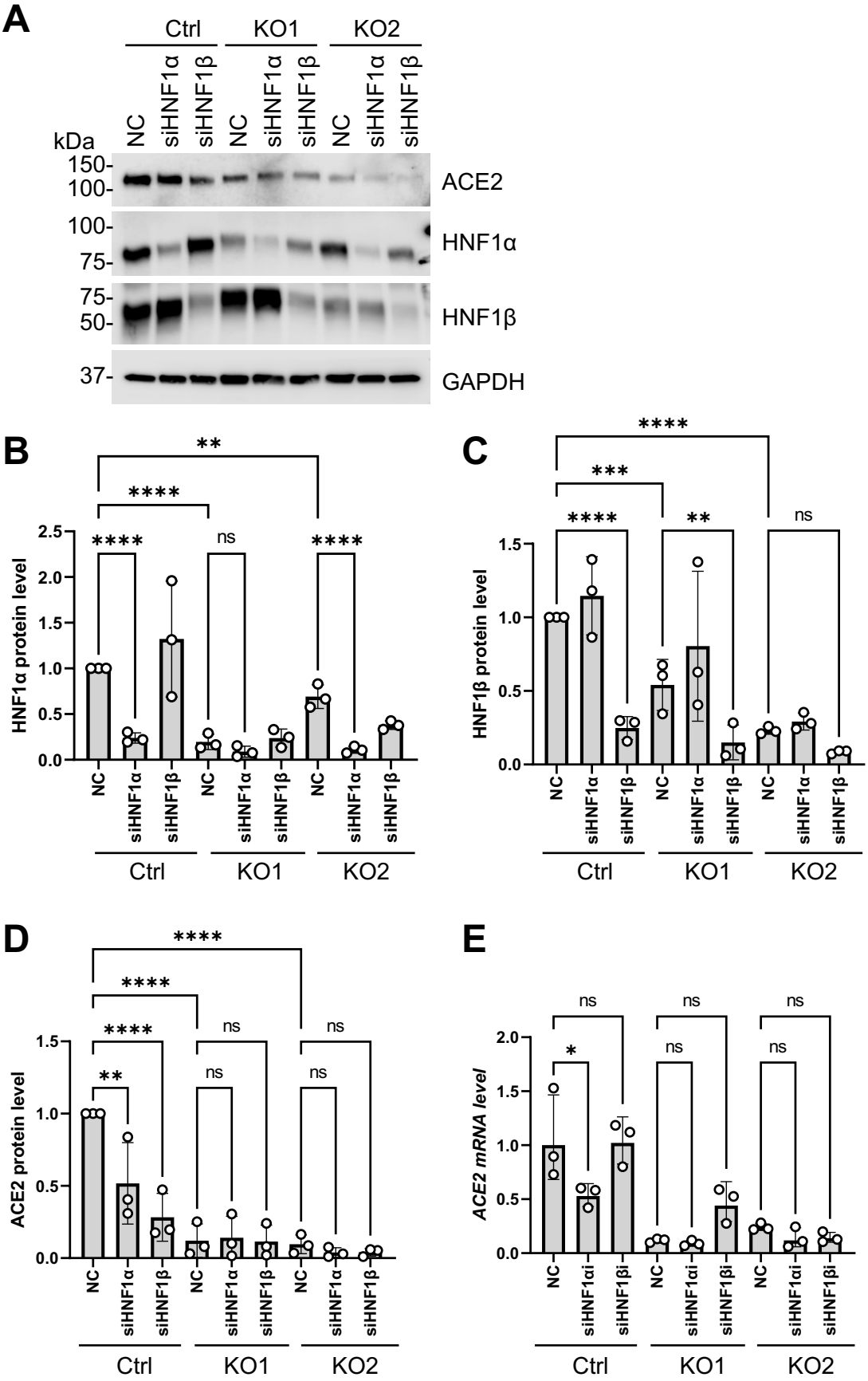
A
Ctrl
KO1
KO2
NC
siHNF1α
siHNF1β
kDa
150-
100-
ACE2
100-
75-
HNF1α
75-
50-
HNF1β
37-
GAPDH
B
HNF1α protein level
C
HNF1β protein level
D
ACE2 protein level
E
ACE2 mRNA level
siHNF1αi
siHNF1βi
ns

Fig. 9

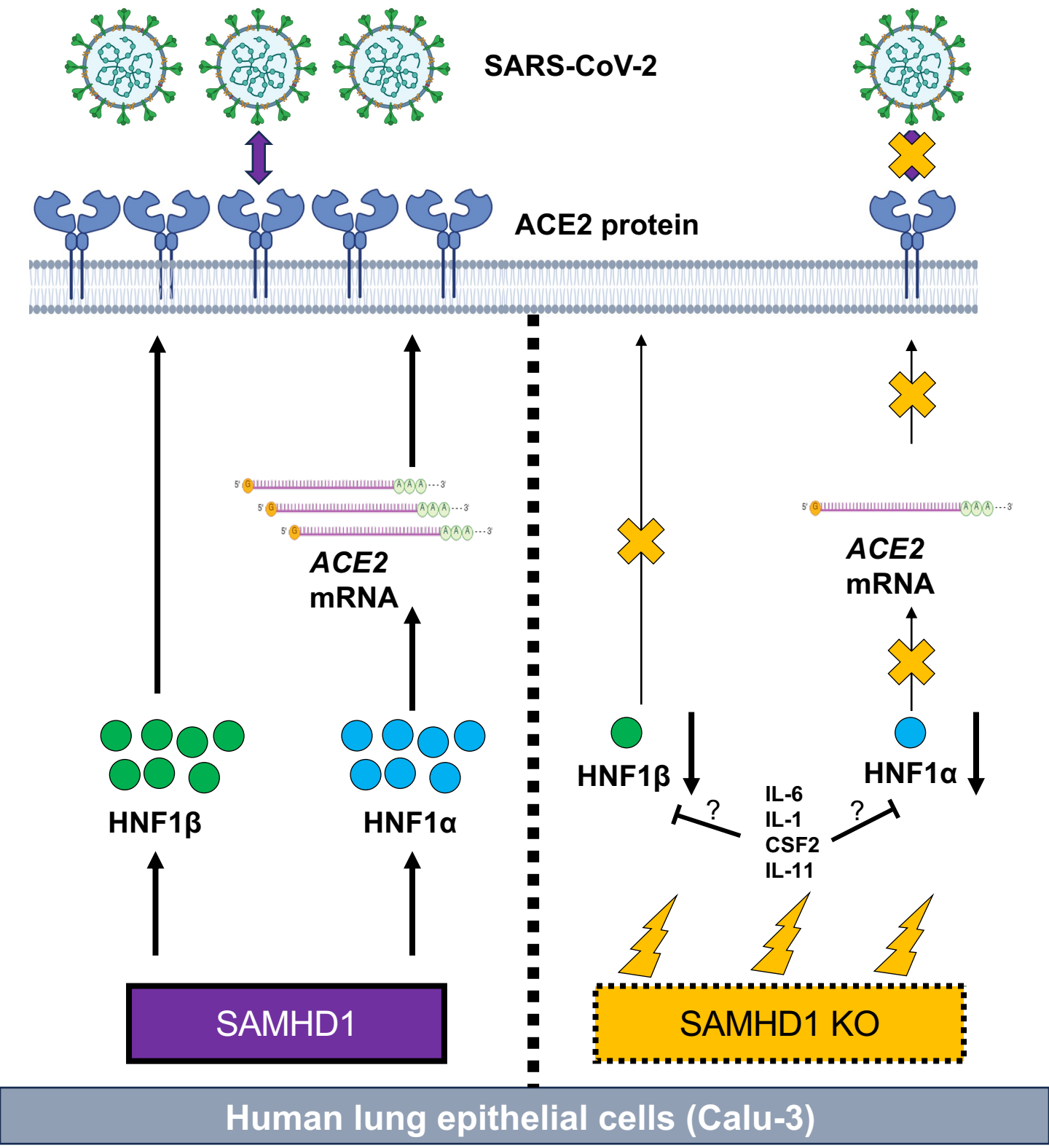
SARS-CoV-2
ACE2 protein
ACE2
mRNA
HNF1β
HNF1α
SAMHD1
ACE2
mRNA
HNF1β
HNF1α
?
?
IL-6
IL-1
CSF2
IL-11
SAMHD1 KO
Human lung epithelial cells (Calu-3)

Supplementary Fig. S1

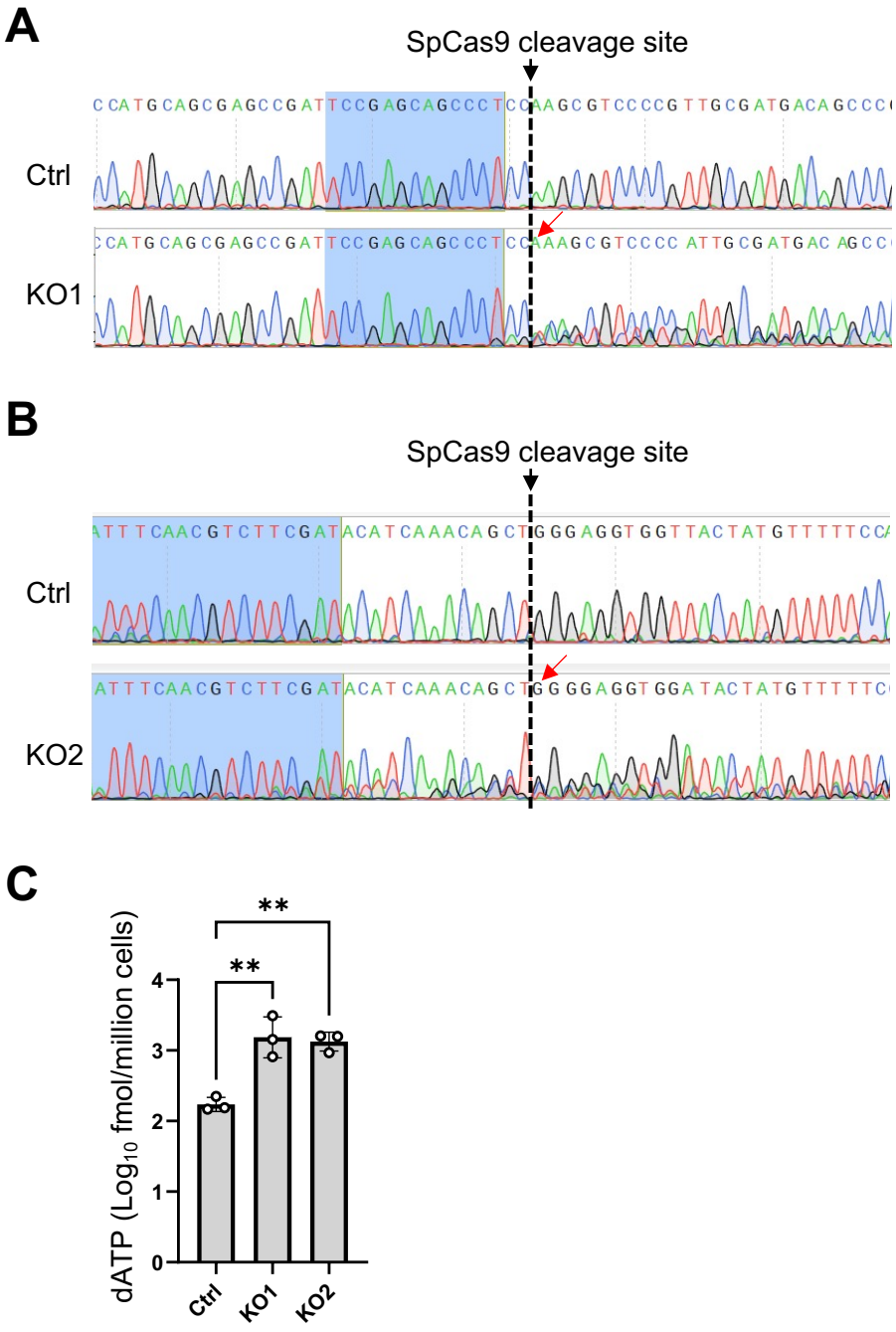

Supplementary Fig. S2

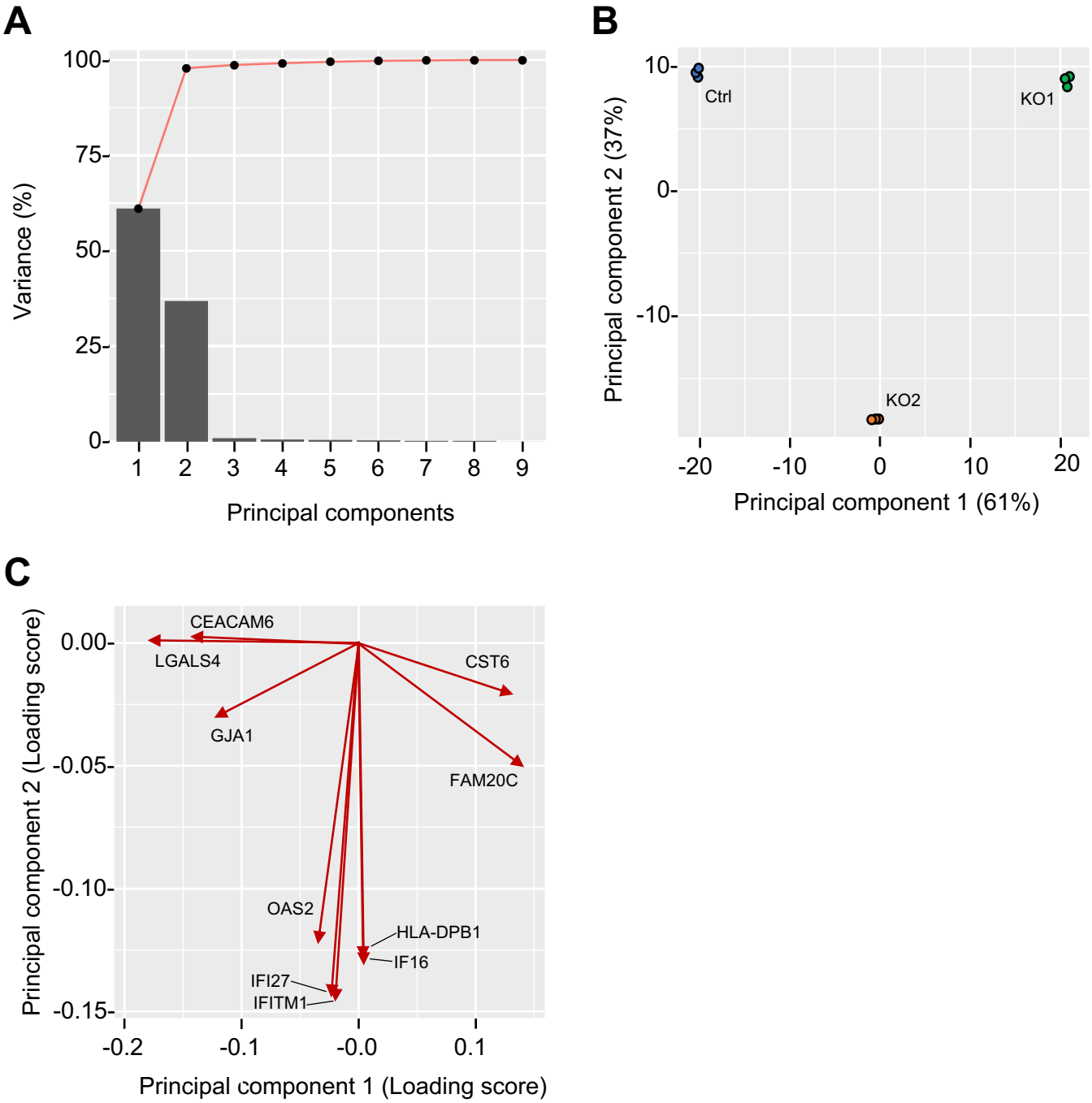

Supplementary Fig. S3

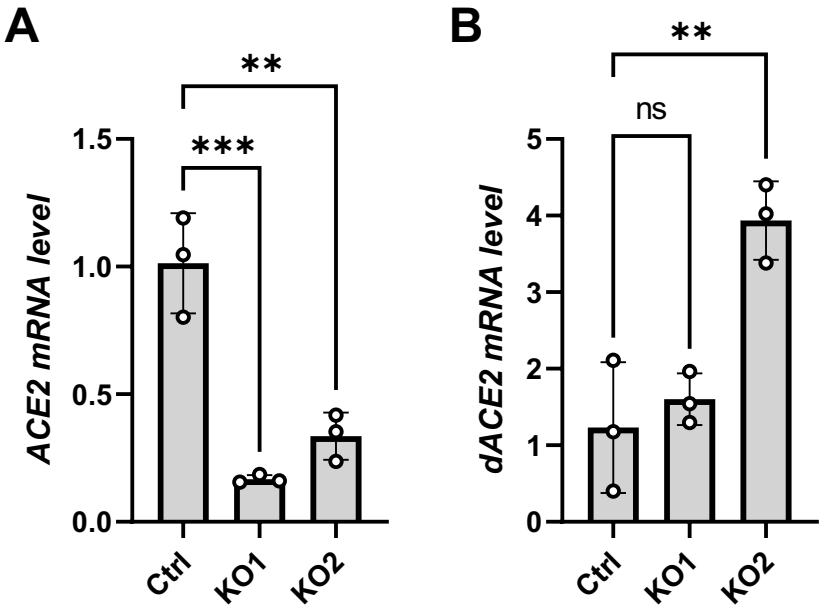

Supplementary Fig. S4

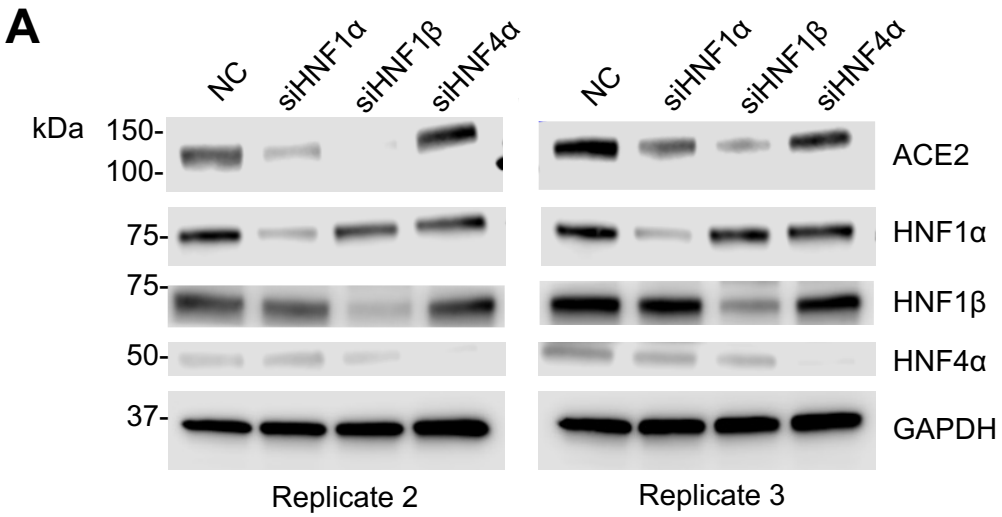

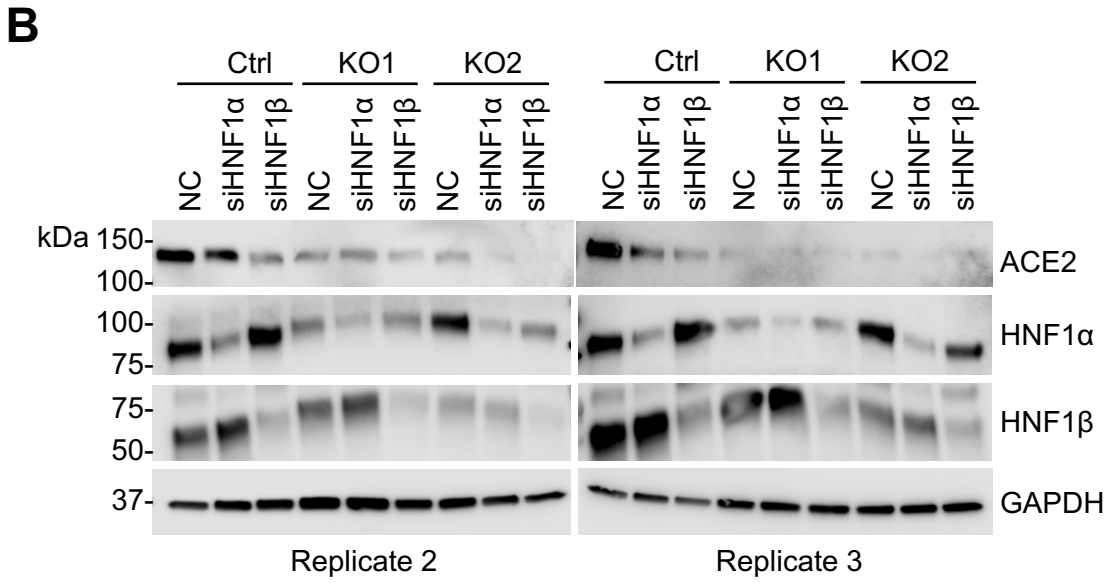
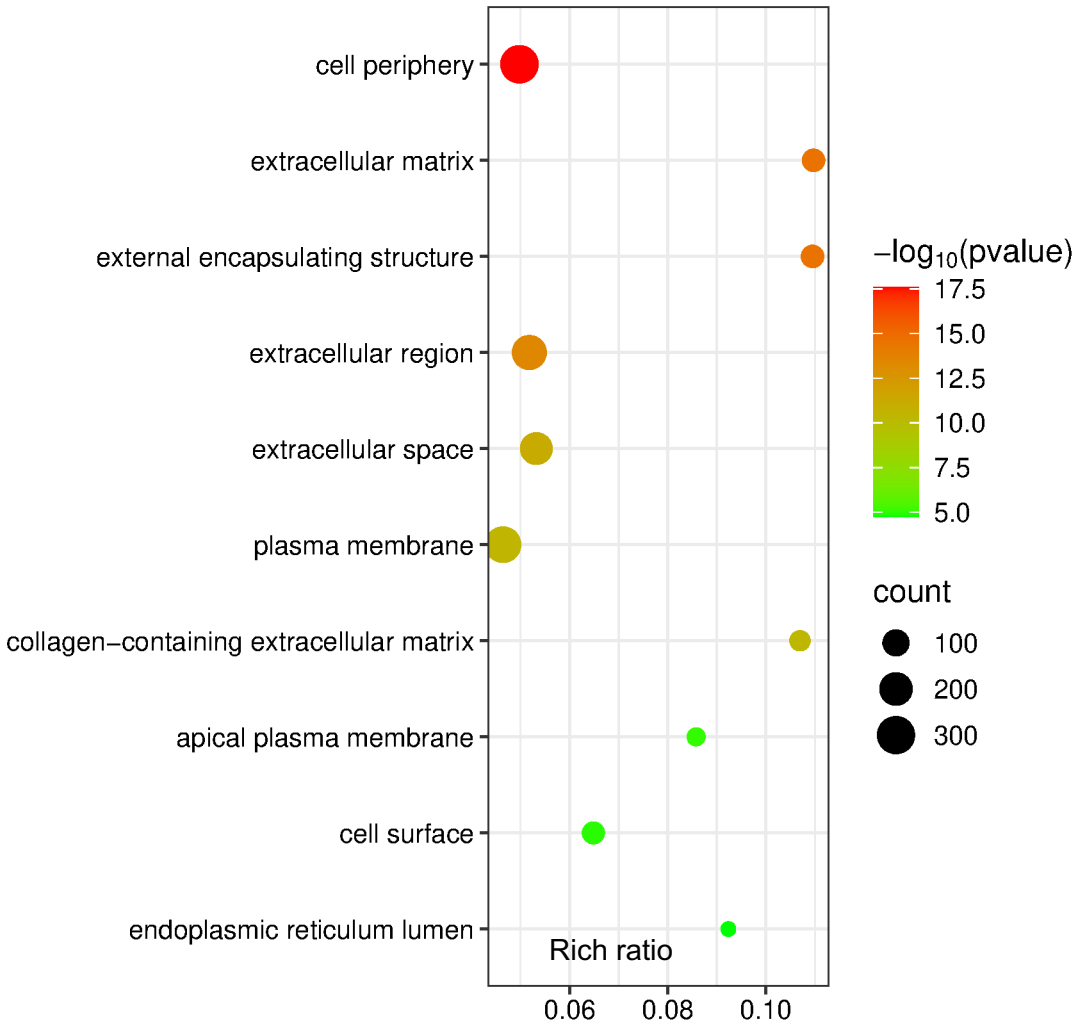
Supplementary Fig. S5